Case Studies in Construction Materials 23 (2025) e05288

Contents lists available at ScienceDirect

Case Studies in Construction Materials

journal homepage: www.elsevier.com/locate/cscm

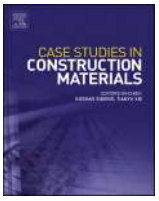

Chemical reactivity of zeolitized volcanic waste materials from Sardinian quarries in the production of eco-friendly pozzolanic mortars for their sustainable recovery

Stefano Columbu [a,*], Davide Comboni [b], Giacomo Diego Gatta [b], Dario Fancello [a], Concetta Rispoli [c], Piergiulio Cappelletti [c], Sara Marrocu [a], Giovanni Brodu [a]

[a] Department of Chemical and Geological Sciences, University of Cagliari, Italy
[b] Department of Earth Sciences, University of Milano, Italy
[c] Department of Earth, Environmental and Resource Sciences, University of Napoli, Italy

ARTICLE INFO

Keywords:
Pozzolanic mortar
Hydrated lime
Cement
Concrete
Waste
Sustainable materials
Construction
Geomaterials

ABSTRACT

The aim of this study is to verify the chemical reactivity between calcium hydroxide $Ca(OH)_2$ and 26 volcanic rocks from different quarry wastes and outcrops of Sardinia to assess their potential use as pozzolans in mortar production and their sustainable recovery in construction materials field. The rocks were analysed from a chemical-mineralogical-petrographic point of view using transmitted light optical microscopy (OM), scanning electron microscopy (SEM), X-ray diffraction (XRD), multiple thermal (TGA–DTA) analyses. In addition, petrophysical (porosity, real and bulk densities, water absorption, etc.) and mechanical tests (compressive, flexural and Point Load strengths) were determined on the experimental mortars made up with the more reactive selected pozzolans. The volcanic rocks are characterised by a highly variable content of glass (from 5 % to 99 vol%) that strongly influences the chemical reactivity with lime, and by the presence of zeolites that may affect the lime-reaction. The results show that the pozzolans here studied exhibit highly variable reactivity with hydrated lime, as function on their compositional and microstructural features. The reactivity of pozzolans is primarily influenced by (i) weight fraction (variable between 5 % and 99 vol%), microstructure and hydration degree of the amorphous matrix, (ii) microporosity and specific surface area; and (iii) chemical-mineralogical alteration of the rock. The most reactive samples have a glassy microstructure with characteristic concentrically trending micro-cracks, or a diffuse microporosity made up by interconnected pores (mainly <10 microns in size). Samples with intermediate or poor reactivity contain moderate to low fractions of glass or exhibit significant mineralogical variability. Rock alteration negatively affects reactivity by forming secondary phases, which reduce the glass-to-mineral ratio. Furthermore, the presence of zeolites, clay-minerals, dolomite and calcite in both pyroclastites and perlitic facies, negatively affects the reactivity. Among the perlites samples, those with a devitrified matrix and secondary minerals (e.g., Ca-erionite) show particularly low reactivity. This study confirms that several volcanic lithologies in Sardinia can be exploited as raw materials for the production of pozzolanic mortars, thanks to their low production cost. In the cement industry, highly reactive pozzolans can (i) bond with portlandite produced during Portland cement hydration (ii) reduce clinker production, thereby lowering gas emissions, and (iii) decrease binder production costs by partially using low-cost raw materials from quarries or industrial waste.

* Corresponding author.
E-mail address: columbus@unica.it (S. Columbu).

https://doi.org/10.1016/j.cscm.2025.e05288
Received 24 March 2025; Received in revised form 26 July 2025; Accepted 9 September 2025
Available online 11 September 2025

1. Introduction

The term *'pozzolan'* is a geomaterial that imparts hydraulic properties to an aerial lime, through pozzolanic reactions that lead to the formation of C-A-S-H phases or gel [1]. Natural pozzolans generally are incoherent or poorly welded volcanic sands (e.g., tuffs, pumice-cineritic pyroclastites), commonly rich in amorphous content. The use of pozzolan dates back to pre-Roman times [2], in which there were its large-scale diffusion, extraction and probable trade between Mediterranean countries [3–7].

The product of lime-pozzolan mixing, known as "Roman cement", enabled the construction of monuments and other infrastructures that have survived remarkably well for over two thousand years (e.g., Pantheon in Rome, Villa Adriana in Tivoli) [8–11]. Among ancient pozzolanic materials, weakly zeolitic pyroclastites should be noted, as they can sometimes positively influence mortar consolidation [12–14]. According to [15], the high specific surface area, cation content, and remarkable cation exchange properties of zeolitic phases promote a faster pozzolanic reaction during the initial setting phase (measured in hours). Materials with Pozzolanic

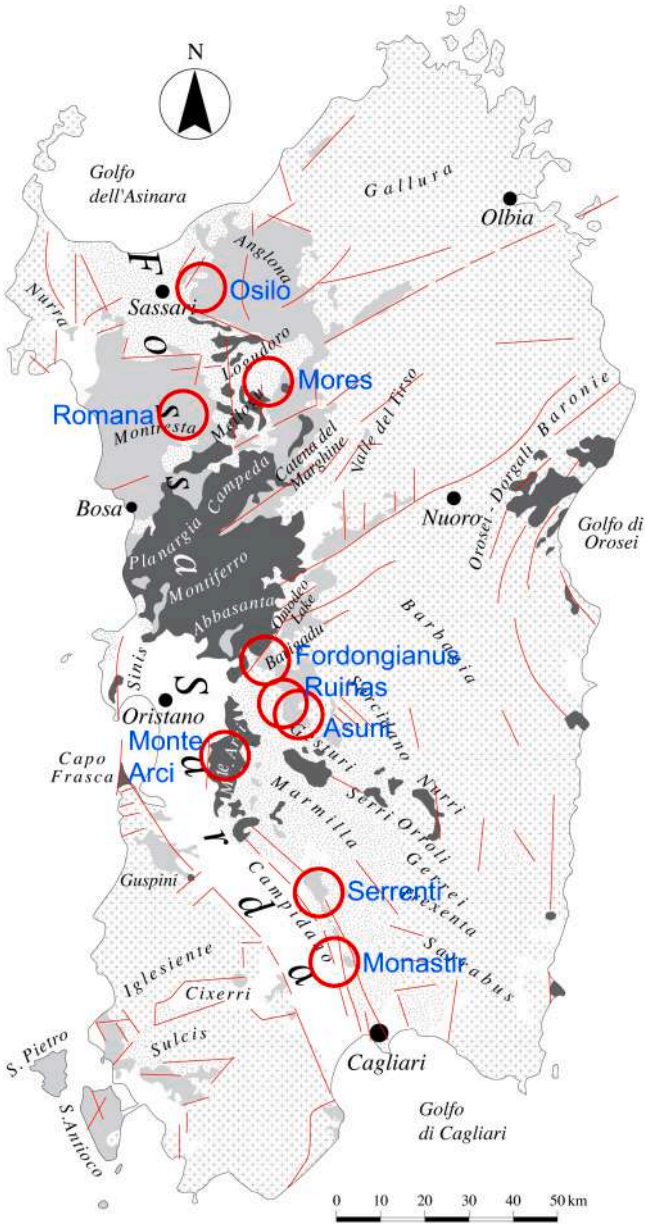

Fig. 1. Schematic geological map of Sardinia with the localization of the sampled rocks. The legend includes patterns and colours corresponding to the lithologies: white = recent alluvial sediments; light grey = Oligo-Miocene volcanic formations including the Oschiri ignimbrites; dark grey = Plio-Pleistocene volcanic formations; stippled grey = Miocene marine sediments; grey crosses = Paleozoic crystalline basement and Mesozoic formations; red continuous and dashed lines = faults (from [40], modified).

Activity (MAPs) fall into the broader class of Supplementary Cementitious Materials (SCMs), which also includes blast furnace slag and some types of fly ash, all of which have intrinsic binding properties [16]. The reactivity of MAPs with lime depends on several factors such as concentrations of silica and alumina, mineralogy, amorphous component, texture, etc. Therefore, premixed MAPs based on lime and pozzolan represent an important resource in the production of hydraulic mortars, both for their technical properties and, above all, for their unquestionable compatibility with the historic built environment [17]. MAPs-based hydraulic limes can replace cement in many cases, providing plasters or mortars with improved thermo-hygrometric regulation (e.g., greater breathability, dehumidifying capacity, insulation), and thus ensuring optimal and balanced microclimatic indoor conditions [18].

Thanks to countless studies concerning the complex chemical-physical aspects of the reaction mechanisms underlying the hardening processes of ancient and modern mortars [19–22], binder production technologies have undergone a great improvement in the last decades [23,24]. Although Portland cement and its derivatives remain the most widely used hydraulic binders, in recent years, mortars made from lime and various types of pozzolans (especially natural), have become increasingly important as raw materials in the construction and restoration of historical buildings [25–28]. This is mainly due to their better compatibility with the stone substrate, their eco-sustainability and to their eco-friendly nature.

The main goal of this research is to test an experimental lime-based pozzolanic mortar with a low environmental impact reuse as fine aggregate the waste materials from volcanic stone quarry of Sardinia. The intent is to experiment with a mortar with excellent hydraulic and physical-mechanical characteristics, classifiable within the commercial category of Formulated Lime mortars (FL), suitable for use in both modern and historical buildings. Thus, twenty-six volcanic rocks coming from selected Sardinian volcanic outcrops (i.e., Morgongiori, Asuni, Ruinas, Fordongianus, Serrenti, Romana, Osilo, Mores and Monastir), formed during the Cenozoic magmatic activity were studied. To define the intrinsic features of the rocks, showing different geochemical and petrographic compositions, and define their reactivity behaviour with lime, several laboratory analyses were made. Firstly, the mineralogical, petrographic, physical (i.e., real and bulk densities, porosity, water absorption and saturation indexes) and mechanical properties (punching, flexural and compressive strengths) of volcanic rocks were studied by Scanning Electron Microscopy (SEM), X-Ray Diffraction (XRD) analyses, Thermo-Gravimetric Analyses (TGA), Helium-picnometry and physical-mechanical Point Load Test (PLT). Then, the chemical reactivity between the slaked lime [i.e., calcium hydroxide $Ca(OH)_2$] and the volcanic rocks, characterized by a glass fraction between 15 and 95 wt%, and zeolites was studied. Lastly, to test the technical performances of the experimental hydraulic mortar, different mixtures were prepared using a slaked lime as binder, a standardised quartz-silicate sand as aggregate and the most reactive volcanic rocks as addictive pozzolanic material. The physical-mechanical properties (PLT index, flexural and compressive strengths) were determined on obtained pozzolanic mortar samples.

2. Geological setting

2.1. Cenozoic volcanism in Sardinia

The sampled rocks of this study come from the Sardinian Oligo-Miocene trough (Fig. 1), a large tectonic depression that crosses Sardinia from North to South [29–33], where an intense igneous activity occurred. It is generally associated with a N-NW directed subduction of oceanic lithosphere beneath the Paleo-European-Iberian continental margin, which likely began in the Middle to Late Eocene and led, during the Oligocene, to the formation of the rift between Sardinia and Provence [34–36]. Cenozoic volcanism is divided in two main following phases, often spatially overlapped but distinct in time and magmatic affinity [34,37–39]:

1) Orogenic magmatic activity, including tholeiitic, calcalkaline, shoshonitic and ultrapotassic lithologies, which formed primarily during Late Eocene–Miocene (~38–15 Ma). The first occurrence of Sardinian orogenic magmatism, dated back to 38.28 ± 0.26 Ma [41], is a small outcrop in the Calabona area in Northern Sardinia (N Sardinia, Fig. 1). Subsequent phases were identified, at the same time, in the area of Alghero (32.3 ± 1.5 Ma; [42]) and Osilo (31.2 ± 1.1 Ma; [42]), as well as in the Southern part of the Island, in the Cixerri area (30.2 ± 0.9 Ma; [43,44]) featuring andesitic lava, dacite domes and rare hypoabyssal bodies. Starting from 22 Ma [43, 45–47], a highly explosive fissural activity produced abundant pyroclastic dacitic-rhyolitic products, alternated with basaltic and andesitic lavas. The volcanic activities occurred in various areas of Sardinia, mainly along the Western graben trending N-S (Fig. 1).

2) Anorogenic magmatism, characterized by tholeiitic to Na-alkaline rocks, which took place during the Late Miocene–Quaternary (~12 to ~0.1 Ma), and geochemically unrelated to active or recent subduction processes [39,41,48]. The activity occurred between ~6 to < 0.1 Ma [34,39,43,49], starting from the Southern sector of Sardinia only (Capo Ferrato, Rio Girone and Guspini; [48,50]). This volcanism produced a range of lithologies, from mafic to silicic, including subalkaline, transitional, and Na-alkaline rocks, sometimes with a K-affinity [49].

3. Materials and methods

3.1. Sampling

Rocks from eight different volcanic fields (from South to North of Sardinia), linked to the Cenozoic magmatism, were sampled (Fig. 1): 1) Monastir (South-West), 2) Serrenti (South), 3) Morgongiori (Mt. Arci, Central-West of Sardinia), 4) Ruinas and Asuni, 5) Fordongianus (Central-West), 6) Romana (North-West), 7) Mores (Central-North) and 8) Osilo (North-West). A total of 26 samples (labelled as CPZ) were collected from outcrops and/or stone quarries (Fig. 2, Table 1): 10 samples from the Mount Arci complex (labelled as CPZ1, CPZ2a, CPZ2b, CPZ3a, CPZ3b, CPZ4, CPZ5, CPZ6, CPZ7, CPZ8), sourced from the Mt. Sparau perlite quarry (Morgongiori) of the Imerys company; 2 samples from the Asuni-Ruinas area (CPZ9, CPZ10), obtained from the Asuni (now inactive)

and Ruinas quarries (owned by Fratelli Frau); 2 samples from Fordongianus (CPZ11a, CPZ11b), collected from the Mura quarry; 1 sample from Serrenti (CPZ12), sourced from Mt. Atzorcu within the 'Sarda Trachiti' quarry; 5 samples from Romana, taken from field outcrops (CPZ13a, CPZ13b-s, CPZ13b-a) and the kaolinite quarry (CPZ14a, 14b); 3 samples from Osilo, sourced from a quarry East of Osilo village (CPZ15a, CPZ15b) and from the Capurru quarry near the village (CPZ17a); 1 sample from Mores (CPZ18), taken from the Mt. Birisone 'Badu e Giaga' locality; and 2 samples from Monastir, collected from the D.O.S. quarry at Mt. Oleadri (CPZ20a) and from Mt. Zara (CPZ20b).

3.2. *Petro-volcanological features of the investigated volcanic sectors*

Excluding the Mt. Arci, which belongs to the Sardinian miocenic-pleistocenic anorogenic magmatism (12–0.1 Ma), the other sampled volcanic sectors are linked to the orogenic volcanic activity (38 and 15 Ma).

Mt. Sparau quarry (where CPZ1–8 samples were taken) belongs to the Mt. Arci (Morgongiori), an important pliocenic volcanic complex (3.8–2.8 Ma), located in Central-Western Sardinia (Fig. 1) including several lava flows and subordinated pyroclastic formations (Fig. 2). It is mainly composed of a subalkaline sequence evolving from subalkaline basalt to rhyolite, with minor transitional basalts (low silica-oversaturated alkali-trachyte) and sporadic alkali-basalts. According to [51,52], the pliocenic stratigraphy consists of (from bottom to top) rhyolitic, dacitic, alkali-trachytic, basaltic and andesitic lava flows. Besides some small outcrops of pyroclastic pumice fall deposits (e.g., Scala Antruxoni locality), the rhyolitic flows mainly consist of (from bottom to top) obsidian, obsidian-perlite, perlite and vesicular flow-banded glassy rhyolite.

The Fordongianus, Ruinas, and Asuni sectors (CPZ9–11), belonging to the oligo-miocenic volcanic-sedimentary succession of the Central Sardinia (Fig. 1), consist of ignimbritic units, mostly emplaced in sub-aerial environments that extend over 200 km^2 for about 300 m in thickness [53]: two lowermost rhyolite-rhyodacite ignimbrites (e.g. Luzzana and Allai units), mainly with hydromagmatic explosive activity, and several uppermost dacite ignimbritic sequences (e.g. Samugheo, Ruinas and Monte Ironi units). The ignimbritic

Fig. 2. Macroscopic features of the sampled pyroclastic rocks: (a-h) rhyolites (samples CPZ2b, CPZ3a, CPZ3b, CPZ5, CPZ6, CPZ7, CPZ8) from Mt. Arci (Morgongiori); (i) rhyolite (sample CPZ13bS) from Romana; (K) rhyodacite/rhyolite (sample CPZ15b) from Osilo; (l) rhyodacite/rhyolite (sample CPZ18) from Mores; (m) andesite (sample CPZ20b) from Monastir. White bar = 4 cm.

Table 1
List of the volcanic samples taken from Sardinian territory.

Sample	Sardinia sector	Locality	Rock type	Volcanic phase
CPZ1	Central-western	Morgongiori	Rhyolite (perlitic)	Miocene-Pleistocene anorogenic
CPZ2a, 2b	Central-western	Morgongiori	Rhyolite	Miocene-Pleistocene anorogenic
CPZ3a, 3b	Central-western	Morgongiori	Rhyolite	Miocene-Pleistocene anorogenic
CPZ4	Central-western	Morgongiori	Rhyolite	Miocene-Pleistocene anorogenic
CPZ5	Central-western	Morgongiori	Perlite (perlitic)	Miocene-Pleistocene anorogenic
CPZ6	Central-western	Morgongiori	Rhyolite	Miocene-Pleistocene anorogenic
CPZ7	Central-western	Morgongiori	Rhyolite	Miocene-Pleistocene anorogenic
CPZ8	Central-western	Morgongiori	Rhyolite (perlitic)	Miocene-Pleistocene anorogenic
CPZ9	Central	Asuni	Rhyodacite/Rhyolite	Eocene-Miocene orogenic
CPZ10	Central	Ruinas	Rhyodacite/Rhyolite	Eocene-Miocene orogenic
CPZ11a, 11b	Central	Fordongianus	Rhyolite	Eocene-Miocene orogenic
CPZ12	Central-southern	Serrenti	Dacite	Eocene-Miocene orogenic
CPZ13a, 13bS, 13bA	North-western	Romana	Rhyodacite/Rhyolite	Eocene-Miocene orogenic
CPZ14a, 14b	North-western	Romana	Rhyodacite/Rhyolite	Eocene-Miocene orogenic
CPZ15a, 15b	North-western	Osilo	Rhyodacite/Rhyolite	Eocene-Miocene orogenic
CPZ17a	North-western	Osilo	Rhyodacite/Rhyolite	Eocene-Miocene orogenic
CPZ18	North-western	Mores	Rhyodacite/Rhyolite	Eocene-Miocene orogenic
CPZ20a, 20b	Central-southern	Monastir	Andesite	Eocene-Miocene orogenic

units are locally interbedded with subordinate andesitic lavas and with the Asuni volcano-sedimentary complex deposits that mainly emplaced in sub-aqueous environments.

The Monastir-Serrenti-Furtei district (samples: CPZ12, CPZ20a, 20b) is connected to the Miocene volcanic activity in the CentralCentral-South Sardinia (Fig. 1) (25.5–23.6 Ma; [43]), in which (from oldest to youngest) andesitic lavas, pyroclastic products, andesitic-basaltic lavas, breccias, epiclastites, peperites were produced [54].

The Romana (samples: CPZ13a, b-S, b-A and CPZ14a, b) and Mores fields (CPZ18) belong to the oligo-miocenic volcanism in Logudoro (North-West Sardinia, Fig. 1) within the Northern part of the Sardinian Rift, which consists of several basin systems, evolved in several phases between the Upper Oligocene and Middle Miocene (and reactivated later in the Pliocene). In this rift area, volcanic activity generated andesitic rocks (about 26 Ma), welded and rheomorphic rhyodacitic to rhyolitic ignimbrites (about 22 Ma), and terminal pyroclastites (20–18 Ma) with associated epiclastic deposits [31,55,56]. Flow-domes, from andesitic to rhyodacitic in composition, close the volcanic sequence, followed by Miocenic volcano-clastic and marine deposits [30].

In the Osilo area, the Oligocene-Miocene volcanic sequence is dominated by high K-calc-alkaline affinity rocks [57], largely made up by porphyritic andesitic flows and intercalated tuffs, with a total thickness exceeding 300 m. Rhyolitic pyroclastic deposits, hosting important epithermal vein mineralization in the NorthWest area, occur in the upper part of the sequence. Late Miocene sedimentary rocks occur sporadically to the West and South, and overlie the Oligocene-Miocene volcanic succession.

3.3. Methods

3.3.1. Mineralogical and petrographic investigations

Petrographic features (e.g., mineralogical phases, microstructural and textural characteristics) of the sampled volcanic rocks and experimental mortars (produced using a lime binder, standard sand as aggregate, and selected pozzolanic volcanic rocks as additives) were studied under a polarizing optical microscope in transmitted light (OM-TL) at various magnifications (1.5X to 40X) on thin sections. This analysis aimed to define textural and microstructural characteristics, to unveil microstructural discontinuities (e.g., micro-cracks, fractures), and to describe the microporosity (e.g., open or closed porosity) of the materials under investigation.

X-ray diffraction data on polycrystalline samples were first performed for a qualitative phase analysis, at the Department of Chemical and Geological Sciences (University of Cagliari, Italy). A PANalytical X'Pert Pro diffractometer (Malvern-PANalytical, Almelo, Netherland) was used, operating in θ-θ geometry and with Ni-filtered Cu-*K*α radiation, equipped with a Real Time multiple strip (RTMS) X'Celerator detector. Data collection conditions were: 5–70° 2θ-range, step-size 0.008° 2θ, 0.19 s per step, 40 kV and 40 mA. Data were processed by the X'Pert HighScore Plus (TM) 2.1.2 software and using the PDF2 database (release 2010 by ICDD, Newtown Square, PA, USA).

A second set of data was collected at the Earth Sciences Dept. – University of Milan, for the quantitative phase analysis of the volcanic rocks, including the amorphous fraction. The samples were first ground in an agate mortar. Then, 14–17 wt% of corundum (α-Al_2O_3) powder was added as an internal standard. The samples were then placed in a back-mounting sample holder, to minimize preferential orientation. A PANalytical X'Pert Pro diffractometer was used, equipped with a X'Celerator detector. The operating conditions for the data collections were: Ni-filtered Cu-*K*α radiation, 40 kV and 40 mA, θ-θ geometry, 2θ-range between 5 and 80°, step size of approximately 0.033° 2θ and a counting time of 60 s per step, under constant temperature (22 ± 1 °C) and humidity conditions (60 %). After the phase identification using the aforementioned same protocol, quantitative phase analysis was performed by the Rietveld method with the GSAS package [58] and the EXPGUI interface [59], following the guidelines of Gualtieri et al.*ii* [60]. The employed starting structural model of the crystalline phases were obtained from the *American Mineralogist Crystal Structure Database* (https://rruff.geo.arizona.edu/AMS/amcsd.php). Full-profile fitting was carried out over the entire collected 2θ range. A Chebyshev polynomial up to 20 coefficients was used to model the background. The peak profile was refined using a Thomson-modified

pseudo-Voigt function, with the peak cut-off set at 0.1 % of the peak maximum. Effects due to preferred orientation of the crystallites were found to be not significant. Unit-cell parameters, average crystallite size, scale factor of each crystalline species, zero shift, and Chebyshev function parameters were refined during the full-profile fit. Atomic coordinates and displacement parameters were fixed to those reported in the literature. For all the samples, convergence was achieved with final good values of the statistical parameters (all having *wRp* < 8 % and *GooF* between 1.2–1.6).

SEM analyses were performed on ten selected samples using a Quanta Fei 200 microscope equipped with a ThermoFischer Ultradry EDS detector, at the CeSAR laboratories (University of Cagliari, Italy). Raw samples were put into the sample chamber without conductive coating to preserve them for further analyses. Therefore, low-vacuum conditions (0.3–0.5 torr) were used to dissipate electrons from incident beam. Variable spot sizes of 4–5 (in arbitrary units given by the Quanta Fei equipment) and accelerating voltage 15–25 kV were adopted during the analytical sessions.

Thermogravimetric analyses (TGA) were performed at atmospheric pressure using a Perkin Elmer device (model TGA7), under Ar flow (60 mL/min). Samples of 10 mg were placed in platinum crucibles and heated from 30 to 900 °C with a heating rate of 10 °C/min. The instrument was calibrated with Curie points of Alumel, nickel, Perkalloy, and iron standard samples, and the temperature was measured with an accuracy of ±2 °C.

Differential scanning calorimetry (DSC) measurements were performed at atmospheric pressure using a DSC7 Perkin Elmer device, under Ar flow (60 mL/min). Samples of 5 mg were placed in platinum crucibles and heated from 30 to 650 °C with a heating rate of 10 °C/min. The DSC7 instrument was calibrated by measuring the melting temperature of metallic indium and zinc (99.999 mass% purity); temperature was estimated with an accuracy of ±0.5 °C.

3.3.2. Reactivity Chapelle test

To test the chemical reactivity of the pozzolan samples with calcium hydroxide, the Chapelle test was adopted. Each sample was finely ground and dried in an oven at 105 °C for 24 h. 1 g of sample was placed into the test tube together with 200 mL of distilled water and 1.26 g of $Ca(OH)_2$, and then was heated on a heating plate at 95 °C for 12 h in a water bath. An open column was placed over the test tube to ensure the dispersion of any gases and to insert the thermometer for temperature monitoring.

The extent of the pozzolanic reaction was calculated by measuring the $Ca(OH)_2$ left in solution after the test by acid titration. The sample-bearing solution was placed in a beaker and phenolphthalein was added, then drops of a HCl 0.1 N solution were added until the colour changed. The result, expressed as mg of $Ca(OH)_2$ per gram of sample, is calculated by difference between the initial and the final concentration.

3.3.3. Mortar specimen production

The experimental mortars were made with different volcanic rocks, which displayed varying reactivity values with $Ca(OH)_2$, as determined by the Chapelle chemical test. Among those, CPZ11a (from the Fordongianus pyroclastite quarry) was found to behave as the most reactive sample, whereas the CPZ13a and CPZ13bS / CPZ14b samples (from the Romana outcrops) showed intermediate and low lime-reactivity behaviours, respectively.

The mortars were produced using a quartz-feldspathic sand as aggregate with grain size ranging between 0.08 ÷ 2 mm (according to the UNI EN 196–1 Standard [61]), slaked (hydrated) lime (with a concentration of $Ca(OH)_2 > 91$ %), selected grounded volcanic rocks (used as pozzolanic aggregate addictive) and water. To homogenize the samples and observe their reactive behaviour with hydrated lime in the mortars, the pozzolanas were preliminarily brought to the same sorted grain size, i.e., < 1 mm, by a jaw crusher and then a ball mill agate. The choice of a not-too-fine grain size arose from the need to physically and mechanically work the pozzolana as an aggregate together with the silicate sand (diameter <2 mm). Considering that the grounded pozzolana was produced without sieving, the ground material used in the mortar mixes presents a good grain size assortment mainly between 80 and 600 μm.

The mortar mixtures were prepared according to the UNI EN 196–1 Standard [61], using the following volumetric proportions of the solid components: 1 portion of binder (i.e., 25 wt% of hydrated lime), 3 portions of aggregate of which 70 wt% sandy silicates and 5 wt% grounded pozzolan. Water was added to the mixture based on a water-to-binder weight ratio of 0.50. The mixtures were then moulded into plastic forms measuring 160 × 40 × 40 mm, in accordance with the [61], for the compression and flexural testing (see Section 3.3.4).

3.3.4. Physical and mechanical tests on rocks and mortars

Physical and mechanical tests were performed on several specimens with different shapes at the Department of Chemical and Geological Sciences (University of Cagliari, Italy) according to the methods described by [62–64]. All the rock samples were previously dried at 105 ± 5 °C to determine the dry solid mass (m_D). The real volume (V_R) of samples sizing 15x15x15 mm was determined by helium Ultrapycnometer 1000 (Quantachrome Instruments) using the following formula:

$$V_R = V_S + V_C$$

where V_S is the solid phases volume of specimens and V_C is the volume of open pores. Then, the wet solid mass (m_W) of the specimens was determined. Using a hydrostatic analytical balance, the bulk volume (V_B) was calculated as:

$$V_B = V_S + V_O + V_C$$

where $V_O = V_B - V_R$ is the volume of open pores and V_B is calculated as:

Table 2
Mineralogical and petrographic features of the volcanic samples as detected by OM-TL and XRD analyses.

Sample	Microscopic description						
	Micro-structure	P.I.%	Phenocrystals (in abundance order)	Texture	Ground mass		Notes
					Type	Crystals	
CPZ1	Porphyritic	2–5	Pl, K-Fds, Op	Fluidal/ eutaxitic	Hypoialine	Pl, Bt, Op, (Px)	Alternating amorphous/crystalline bands
CPZ2a	Porphyritic	2–4	Pl, Sn, Op	Intersertal	Hypocrystalline	Pl, Bt, Op, (Px)	Reddish microplagues (NP)
CPZ2b	Porphyritic	3–5	Pl, Sn, Or, Op	Intersertal/ fluidal	Hypocrystalline	Pl, Bt, Op, (Px)	Iso-oriented reddish microplagues (NP)
CPZ3a	Porphyritic	1–2	Pl, Bt, Op	Fluidal	Hypoialine	Pl, Bt, Op	Blackish elongated shards and 2 mm black-Mca/zeolite microliths (?)
CPZ3b	Porphyritic	3–4	Pl, K-Fds, Bt, Op	Fluidal	Hypocrystalline	Pl, Qz, Op	Iso-oriented irregular micro-fractures and reddish plagues and (2 mm) black-Mca/zeolite microliths (?)
CPZ4	Aphyric	/	/	Vitrophyric	Holoialine	Phy (e.g. Mca)	(1.5 mm) black micronodules (obsidian grains?) and iso-oriented (2 mm) black-Mca/zeolite microliths, perlitic-globular microstructure with spheroidal fractures and iso-oriented porous
CPZ5	Porphyritic	4–5	Pl, Op, Bt	Pseudofluidal	Hypoialine	Pl, Op, Mca, Qz	Perlitic microstructure with spheroidal fractures and globular reddish-brown plagues with inside microcrystals
CPZ6	Porphyritic	5	Sn, (Pl)	Eutaxitic/ fluidal	Hypoialine	K-fds, Op, Qz	Glassy brown micro-bands at different crystallinity and black iso-oriented phases
CPZ7	Porphyritic	2–3	Pl, (K-fds), (Bt)	Fluidal	Hypoialine	Pl, Bt, Op	Blackish iso-oriented shards, porous and 2 mm black-Mca/zeolite microliths
CPZ8	Porphyritic	1–2	K-fds, Bt, (Pl)	Pseudofluidal/ intersertal	Ialine	(K-fds)	Blackish spheroidal glassy micro-shards
CPZ9	Porphyritic	3–5	K-fds (Sn), Qz, (Pl)	Vitrophiric	from ialine to devetrified	rare microliths of Pl, Qz	Abundant shards in ground mass with probable presence of phyllosilicates
CPZ10	Porphyritic	8–9	Pl, K-fds, Qz, (Px)	Pseudofluidal	Hypocrystalline	Pl, K-fds, Qz, Op, (Px)	Abundant elongated pumices, micro-lithics and cognate fragments
CPZ11a	Porphyritic	10–12	K-fds, Pl, Px	Pseudofluidal	Hypocrystalline	Pl, K-fds, Px, Qz, Op	Abundant elongated pumices, magmatic micro-lithics and cognate fragments with greenish matrix (probably consisting of Glc, Cel)
CPZ11b	Porphyritic	6–8	Sn, Pl, Px	Pseudofluidal	Hypocrystalline	Pl, K-fds, Op, Px, Qz	Abundant elongated pumices, magmatic micro-lithics and cognate fragments
CPZ12	Porphyritic	13–15	Pl, Op, Px	Pseudofluidal	Hypocrystalline	Pl, Op, Px, (Qz)	Abundant pumices, lithics and cognate/xeno-fragments
CPZ13a	Porphyritic	9–12	Pl, (K-fds)	Pseudofluidal	Hypoialine/ hypocrystalline	Zeo, Pl, Op, Phy?	Presence of feldspar relicts, microlithics, crystal-clasts
CPZ13bS	Porphyritic	9–12	Pl, Bt, (K-fds)	Pseudofluidal	Hypoialine/ hypocrystalline	Zeo, Pl, Op, Bt	Presence of feldspar relicts, microlithics and crystal-clasts
CPZ13bA	Porphyritic	9–12	Pl, (K-fds)	Isotropic	Hypoialine/ hypocrystalline	Zeo, Pl, Bt	Presence of feldspar relicts, microlithics, crystal-clasts and porous
CPZ14a	Porphyritic	14–18	Pl, K-fds, Bt, Qz	Pseudo-vitrophyric	Hypoialine/ hypocrystalline	Pl, (Bt), (Op)	Flattened and welded pumices, glassy shards
CPZ14b	Porphyritic	14–16	Pl, (K-fds), Bt, Qz	Pseudo-vitrophyric	Hypoialine/ hypocrystalline	Pl, (Bt), (Op)	Flattened and welded pumices, glassy shards
CPZ15a	Porphyritic	35–38	Pl, Qz, (K-fds)	Intersertal/ integranular	Hypocrystalline	Qz, Pl, Mca	High alteration, mainly mineral relicts
CPZ15b	Porphyritic	35–38	Pl, Qz, (K-fds)	Intersertal/ integranular	Hypocrystalline	Qz, Pl, Mca	High alteration, mainly mineral relicts
CPZ17a	Porphyritic	20–25	Pl, Qz	Intergranular	Hypocrystalline/ altered	Pl, Qz	High alteration, mainly mineral relicts and recrystallization
CPZ18	Porphyritic	10–12	Pl, K-fds, Qz	Hypoialine	Pseudo-fluidal	Pl, Qz, Zeo	Abundant elongated pumices, magmatic micro-lithics and cognate fragments
CPZ20a	Glomerulo-porphyritic	30–35	Pl, (Px), (Op)	Intersertal/ integranular	Hypocrystalline	Pl, Op	High alteration, mainly mineral relicts
CPZ20b	Glomerulo-porphyritic	30–35	Pl, Px, Op	Intersertal/ integranular	Hypocrystalline	Pl, Px, Op	High alteration, mainly mineral relicts

Abbreviations: Qz = quartz; K-fds = K-feldspar; Pl = plagioclase; Bt = biotite; Op = opaque mineral; Px = pyroxene; Cel = celadonite; Glc = glauconite; Zeo = zeolite; Mca = mica; Phy = phyllosilicate; P.I. = porphyritic index.

$$V_B = \left[\frac{(m_w - m_{HY})}{\rho_{WT}}\right] \cdot 100$$

where m_{HY} is the hydrostatic mass of the wet specimen and ρ_{WT} is the water density at a temperature of 25 °C. Total porosity (Φ_T), water/helium open porosity ($\Phi_O H_2O$-He), water/helium closed porosity (Φ_C H_2O-He), weight imbibition coefficient (IC_W), saturation index (SI), bulk (ρ_B) and real (ρ_R) densities were computed as:

$$\phi_T = \left[\frac{(V_B - V_S)}{V_B}\right] \cdot 100; \Phi_O\ H_2O = \left\{\frac{\left[\frac{(m_W - m_D)}{\rho_{WTx}}\right]}{V_B}\right\} \cdot 100; \Phi_O\ He = \left[\frac{(V_B - V_R)}{V_B}\right] \cdot 100$$

$$\Phi_C\ H_2O = \Phi_T - \Phi_O\ H_2O; \quad \Phi_C\ He = \Phi_T - \Phi_O\ H_e$$

$$IC_w = \left[\frac{(m_w - m_D)}{m_D}\right] \cdot 100; SI = \left(\frac{\Phi_O H_2O}{\Phi_O H_e}\right) = \left\{\frac{\left[\frac{(m_W - m_D)}{\rho_{WTx}}\right]}{V_O}\right\} \cdot 100$$

$$\rho_S = \frac{m_D}{V_S}; \rho_R = \frac{m_D}{V_R}; \rho_B = \frac{m_D}{V_B}$$

A Point Load Tester (mod. D550 Controls Instrument) was used to determine the resistance to concentrated load (i.e. PLT index (Is)) of rock samples according to ISRM Recommendations [65], was calculated as:

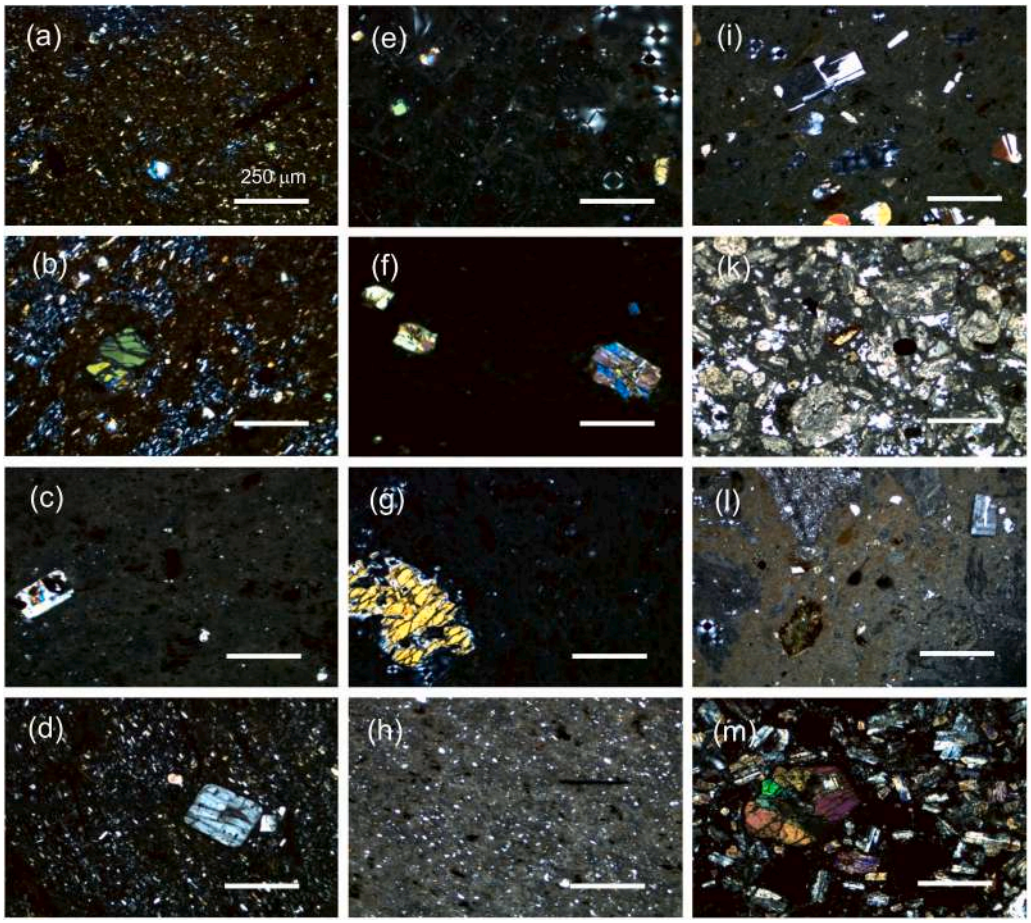

Fig. 3. Comparison between different pyroclastic rocks from Sardinia - microphotographs under crossed polarizers. Rhyolite CPZ2 (a-b) and CPZ3a, CPZ3b, CPZ5, CPZ6, CPZ7, CPZ8 (c-h) from Mt. Arci (Morgongiori); (i) rhyolite CPZ13bS from Romana; (K) rhyodacite/rhyolite CPZ15b from Osilo; (l) rhyodacite/rhyolite CPZ18 from Mores; (m) andesite CPZ20b from Monastir. White bar = 250 µm.

$$Is = \frac{P}{De^2}$$

where P is breaking load and De the "equivalent diameter of the cylindrical specimen" [65] calculated as:

$$De = \frac{4A}{\pi}; A = W \cdot D$$

where W is the width perpendicular to the load direction and 2 L is the length of specimen, and D is the distance between the two conical punches. The index value $Is_{(50)}$) is referred to a standard cylindrical specimen with diameter D = 50 mm, for which it has been corrected with a shape coefficient (F) and calculated as:

$$Is_{(50)} = Is \cdot F = Is \cdot \left(\frac{De}{50}\right)^{0.45}$$

The uniaxial compressive (R_C) and flexural (R_f) strengths of mortars were determined according to the UNI EN 196–1 Standard [61] on prismatic specimens with dimensions 40x40x80 mm and 40x40x160 mm respectively, after drying at a temperature of 70°C to constant mass using a 3000 kN electro-hydraulic press (Controls).

4. Results

4.1. Mineralogical, petrographic and physical characteristics of volcanic rocks

4.1.1. Microscopic features

The analysed samples (CPZ1-CPZ8) from Mt. Sparau quarry (Mt. Arci) are mainly glassy-perlitic and flow-banded rhyolites (Table 2; Fig. 3). The perlite exhibits abundant intersecting, concentric, curvi-planar cracks, generally in sub millimetric size. The samples show a microstructure from aphyric (CPZ4) to porphyritic (CPZ1–3, CPZ5–8, with a porphyritic index (P.I.) ranging from 1 % to 5 %, Table 2, Fig. 3), with (in abundance order) plagioclase, K-feldspar (mainly sanidine) ± biotite phenocrysts (CPZ1, 2a, 2b, 3b, 7, Fig. 3), or with plagioclase ± biotite phenocrysts (CPZ3a, 5), or with sanidine ± subordinate plagioclase (CPZ6), or sanidine ± biotite (CPZ8, Fig. 3h). The texture varies from vitrophyric (CPZ4) to pseudofluidal (CPZ5, Fig. 5, CPZ8, Fig. 3h), fluidal (CPZ3a, 3b, 7), eutaxitic (CPZ1, Fig. 4, CPZ6, Fig. 3f), or pseudo-intersertal (CPZ2a, CPZ2b, Fig. 3a, b). The clearly perlitic lithofacies show spheroidal and curviplanar microfractures. The ground mass, containing plagioclase ± quartz ± biotite ± opaque, zeolites and rare pyroxenes and phyllosilicates, varies from holoialine (CPZ4) to hypoialine (CPZ1, 3a, 5–8), or hypocrystalline (CPZ2a, 2b, 3b).

The rhyodacitic-rhyolitic pyroclastites of Asuni quarry (CPZ9) show a vitrophyric texture and a porphyic structure (P.I. = 3–5 %, Table 2), mainly with quartz ± sanidine and rare plagioclase phenocrysts. The ground mass is ialine with rare and small plagioclase microliths ± opaque, and rare phyllosilicates (Table 3). According to [66,67], the Asuni unit contains secondary mineralization dominated by zeolites.

The rhyolitic rock from the Ruinas quarry (CPZ10) shows a porphyritic structure (P.I. = 3–5 %, Table 2), mainly with plagioclase ± sanidine ± quartz phenocrysts and subordinate opaques and pyroxenes. The texture ranges from pseudofluidal to isotropic, with a hypocrystalline groundmass containing plagioclase, ± opaque minerals, and rare pyroxene.Pyroclastic samples from the Mura quarry of Fordongianus outcrops (CPZ11a, Fig. 6, CPZ11b) have a porphyritic structure (P.I. from 6 % to 8 % in CPZ11b to 10–12 % in CPZ11a, Table 2) with K-feldspar, plagioclase ± quartz, opaques with a pseudofluidal texture and a hypocrystalline groundmass, with plagioclase and rare pyroxene (Tables 2, 3).

The dacitic rocks from Serrenti quarry (CPZ12) show a porphyritic structure (P.I.) about 15 %, with phenocrystals of opaques (likely Ti-magnetite and magnetite), plagioclase (with composition from andesine to oligoclase) ± orthopyroxene, and rare quartz.

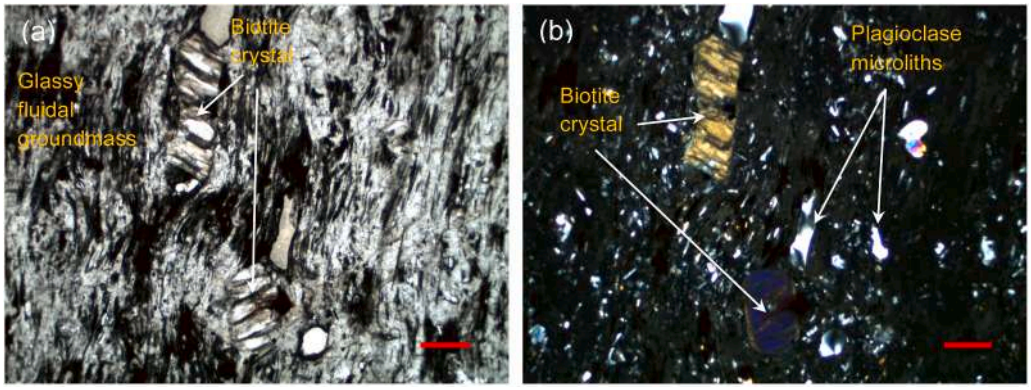

Fig. 4. Microphotographs of rhyolitic pyroclastic rocks CPZ1 from Mt. Arci at parallel (a) and crossed (b) polarizers: biotite crystals within the glassy fluidal groundmass, where plagioclase microliths are present. Red bar = 500 μm.

The groundmass mainly consists of plagioclase microliths.

The pyroclastic rocks of Romana outcrop (CPZ13a, 13bA, 13bS, Fig. 3) show a variable grain size ranging from medium to fine grained, with a porphyritic structure (P.I. from 9 % to 12 %) with phenocrysts mainly of plagiolase from andesine–labradorite composition, often microfractured, or as relic, and rare biotite. The texture is pseudofluidal. The groundmass (ranging from hyaline to hypo-hyaline or hypocrystalline; see Table 2) contains embedded glass shards, lithic and crystal clasts, and rare microliths of plagioclase and black mica (biotite). Sample CPZ13bS shows the presence of zeolite acicular microcrystals into the microcavities of the glassy matrix.

Samples from Romana quarry (CPZ14a, 14b) show a porphyritic structure with a higher porphyritic index (12–16 %) with phenocrystals of plagioclase, K-feldspar ± biotite ± quartz. The texture is pseudo-vitrophyric and the groundmass is from ialine to hypocrystalline, with rare crystals of plagioclase, biotite and opaques. Volcanic rocks sampled from the Osilo outcrop (CPZ15a, 15b, Fig. 3) show a porphyritic structure (P.I. 35–38 %, Table 2) with altered phenocrysts of plagioclase and quartz. Samples show an integranular texture and a hypocrystalline ground mass, with plagioclase and rare mica.

Samples from Capurru quarry (CPZ17) show a porphyritic structure with a lower index (P.I. ~20–25 %), with plagioclase and quartz relic phenocrysts. The hypocrystalline groundmass, including plagioclase and opaques, is very altered. Pyroclastic samples from Mores outcrop (CPZ18, Fig. 3l) have a porphyritic structure (P.I. 10–12 %) with plagioclase, K-feldspar, quartz, opaques, with a pseudofluidal texture and an hypoialine groundmass, characterised by rare plagioclase microliths.

The andesitic rocks from Monastir area (CPZ20a, 20b, Fig. 3m) show a medium-high alteration grade, with a glomero-porphyritic index (P.I. 30–35 %) for phenocrystals of plagioclase and pyroxene, with an intersertal texture and a groundmass with plagioclase ± pyroxene.

4.1.2. XRD analyses

The analysed volcanic rocks show different crystals/glass ratios, with glass content varying from 15 % to 95 % in volume.

In addition to the primary mineralogical phases identified by the OM-TL analysis (Table 3, mineral abbreviations according to [68] (Fig. 7), which mainly include Ca- and Na-plagioclase, K-feldspar (i.e., sanidine, microcline, orthoclase), pyroxene, quartz, opaque minerals and subordinately biotite and amphibole, X-ray diffraction analysis revealed accessory minerals (<7 %) with very fine grain sizes and, therefore, undetectable by optical microscopy. Among these phases (Table 3), zeolites were identified in several samples (CPZ3a, 4, 8, 9, 10, 12, 13a, 13bS, 13bA, 14a, 14b, 18), represented by the following mineralogical species: erionite, laumontite, clinoptilolite, stilbite, and mordenite. Additionally, clay minerals such as smectite, illite, and chlorite were found in samples most affected by alteration processes (CPZ9, 12, 13a, 13bA, 15a, 15b, 17a, 20a, 20b).

4.1.3. Physical properties

The analysis of physical properties such as density, porosity and water saturation (Table 4) was performed to first define the intrinsic characteristics of the investigated pozzolanic materials. In addition, the study of the solid density (i.e., absolute density determined on the powered sample) and the real density (including the helium-closed porosity) can also be useful to indirectly define the mineralogical association, the presence / type of the glass of vulcanites and their porosity.

Based on the analytical data, the samples from Morgongiori, Osilo, Serrenti and Mores exhibit the loWest values of total porosity among all, resulting in the highest apparent density values (Table 4, Fig. 7). In contrast, the Asuni-Ruinas and Fordongianus samples, characterized by very high porosity (ranging from 34 % to 40 %), display low bulk density values.

The vulcanites of Romana, Mores and Morgongiori show low values of bulk density if compared to the vulcanites of Osilo (Fig. 7), Serrenti, Asuni-Ruinas and Fordongianus, corroborated even by a higher helium-closed porosity at least for the Morgongiori, Osilo and Romana samples (Fig. 8). Conversely, the vulcanites from Asuni-Ruinas and Fordongianus show consistently low closed porosity values (< 1.3 %). Consistently with the high helium open porosity, the Asuni-Ruinas and Fordongianus samples have correspondingly

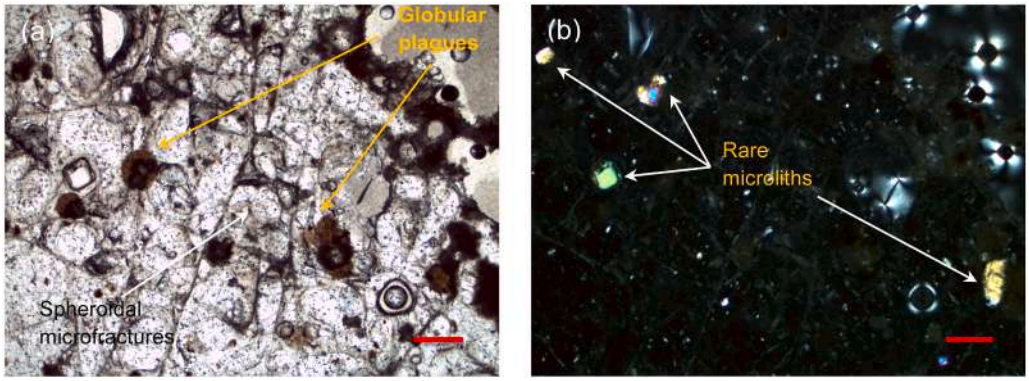

Fig. 5. Microphotographs of rhyolitic pyroclastic rocks CPZ5 from Mt. Arci under parallel (a) and crossed (b) Nicol: hypoialine groundmass with perlitic microstructure, spheroidal microfractures and globular reddish-brown plagues. Rare plagioclase, quartz and biotite microliths occur. Red bar = 500 μm.

Table 3
Mineralogical and glass composition (as wt%) of the volcanic rocks studied in this study, as obtained by the Rietveld full-profile fit (see text for details).

		SIALIC MINERALS								MAFIC MINERALS			ZEOLITE MINERALS					OTHER SUBORDINATE MINERALS					
Sample	**Glass**	**Qz**	**Crs**	**Trd**	**Sn**	**Mcc**	**Or**	**Ab**	**An**	**Aug**	**Amph**	**Bt**	**He**	**CaEr**	**Lmt**	**Stb**	**Clp**	**Mor**	**Mnt**	**Msc**	**Il**	**Chl**	**Dol**	**Cc**
CPZ1	81(3)	0.5 (2)					2.7 (5)	13 (2)				1.80 (7)		1.0 (6)										
CPZ2a	24(2)	13.3 (8)			10.3 (9)	28 (1)		24.7 (9)																
CPZ2b	63(3)	1.8 (5)	10.1 (6)		5.6 (9)		19.6 (1)																	
CPZ3a	82(2)							13.5 (9)				2.1 (9)			2.7 (6)									
CPZ3b	81(3)	0.5 (2)					2.7 (5)	12.8 (15)				1.8 (7)		1.0 (6)										
CPZ4	99(1)													0.1 (1)						0.2 (1)	0.2 (1)			
CPZ5	86(3)		4.7 (7)						8.8 (9)			0.9 (3)												
CPZ6	32(2)	0.70 (4)	18.2 (6)	7.9 (5)	40.9 (14)		0.7 (2)																	
CPZ7	97(3)	1.0 (3)			0.6 (3)							1.0 (3)												
CPZ8	99(1)						0.1 (1)					0.5 (2)		0.2 (1)										
CPZ9	37(3)	18.2 (7)				4.7 (7)	15.2 (12)									0.2 (2)		24.7 (9)	0.3 (1)					
CPZ10	7(1)	20.8 (6)					28 (1)	43 (1)							1.2 (6)									
CPZ11a	23(2)	14.2 (7)			3.3 (1)	40.6 (10)		18.9 (9)																
CPZ11b	5.0 (2)	14.4 (7)			12.4 (10)	44.6 (12)		23.6 (10)																
CPZ12	27(2)							52.5 (5)	7.3 (6)		2.3(6)				10.2 (6)				0.3 (3)					
CPZ13a	33(2)							11.0 (6)									54.0 (5)				2.2 (5)			
CPZ13bS	27(2)							7.2 (9)				11.8 (9)					54.1 (12)							

(*continued on next page*)

Table 3 (*continued*)

		SIALIC MINERALS					MAFIC MINERALS		ZEOLITE MINERALS		OTHER SUBORDINATE MINERALS				
CPZ13bA	21(2)				9.2			1.90		68					
					(9)			(9)		(1)					
CPZ14a	28(3)	11.5		13.3		15.5		3.2		29.3					
		(12)		(12)		(12)		(9)		(12)					
CPZ14b	37(2)	3.0			5.6	9.5		3.7		40.9					
		(5)			(6)	(9)		(6)		(15)					
CPZ15a	39(2)	20.2			13.0						7.5	9.6	11.2		
		(5)			(6)						(10)	(10)	(8)		
CPZ15b	31(2)	17.2			16.2						11.9	12.2	11.9		
		(8)			(9)						(8)	(7)	(9)		
CPZ17a	25(2)	11.6			12.1							42.1		9.3	
		(7)			(8)							(10)		(5)	
CPZ18	33(3)	6.8	7.9			14.3				37.6					
		(5)	(15)			(15)				(10)					
CPZ20a	31(2)	9.9				47.6		3.9			7.3				
		(5)				(7)		(5)			(6)				
CPZ20b	42(2)	3.4				38.7	12.9	2.5			0.9				
		(1)				(9)	(15)	(6)			(5)				

Abbreviation legend: Qz = quartz; Crs = cristobalite; Trd = tridymite; Sn = sanidine; Mcc = microcline; Or = ortoclase; Ab = albite; An = anortite; Aug = augite; Amph = amphibole; Bt = biotite; He = hematite; CaEr = Ca-erionite; Lmt = laumontite; Stb = stilbite; Clp = clinoptilolite; Mor = mordenite; Mnt = montmorillonite; Msc = muscovite; Il = ilmenite = Chl = chlorite; Dol = dolomite; Cc = calcite.

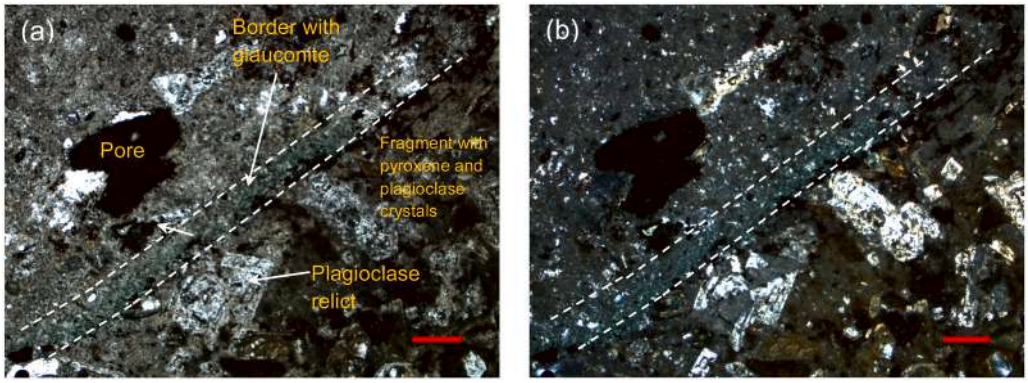

Fig. 6. Microphotographs of rhyolitic pyroclastic rocks CPZ11a from Fordongianus quarry under parallel (a) and crossed (b) polarizers: reddish glauconite zone between the porous glassy matrix (on the left) and fragment (on the right) with plagioclase microliths. Red bar = 500 μm.

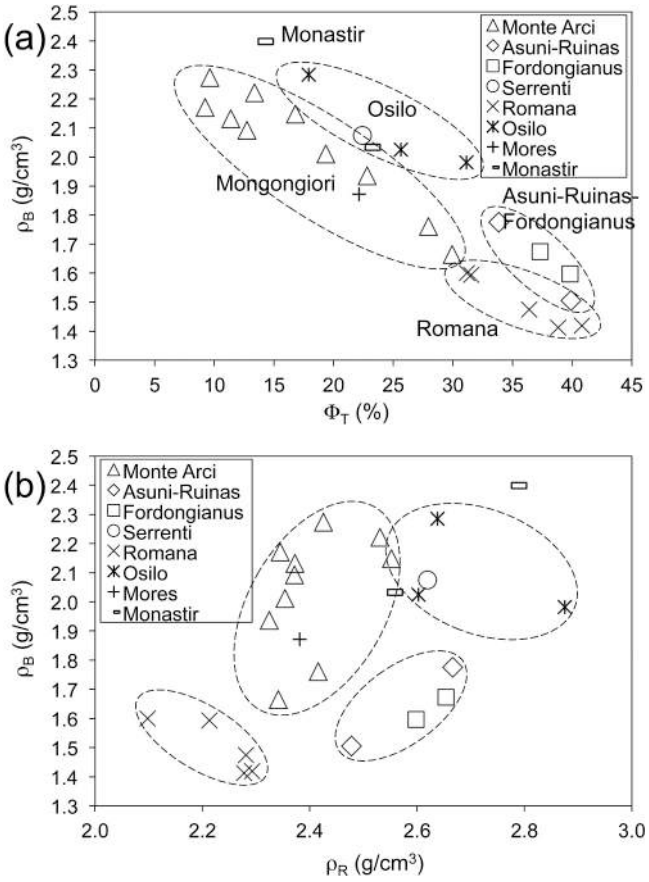

Fig. 7. Physical properties of the Sardinian vulcanites sampled for this study: (a) total porosity vs. bulk density; (b) real density vs. bulk density.

higher water absorption values, as shown by the water open porosity (ϕ_O H_2O: 33–38 %) and imbibition coefficients (IC_W %: 19–25 %; Table 4). The saturation index always remains below the 100 % limit (Fig. 8). Only a few samples, from the Asuni-Ruinas and Fordongianus areas and characterised by high porosity open to water, overlap the 100 % line; this could reflect the occurrence of pores with smaller diameters, allowing an easier absorption of the liquid phase within the porous rock matrix.

4.1.4. Mechanical properties by PLT test

In general, albeit with some exceptions, the mechanical behaviour of the vulcanites, as obtained by the PLT strength index ($Is_{(50)}$, Table 5), substantially reflect the physical properties highlighted in the previous section (see Table 4). For these reasons, variability in

Table 4
Physical properties of pozzolans; ρ_S = solid density; ρ_R = real density; ρ_B =bulk density; Φ_O He = helium open porosity; Φ_C He = helium close porosity; Φ_O H_2O = water open porosity; Φ_C H_2O = water close porosity; Φ_T = total porosity; IC_W = water imbibition coefficient; SI = water saturation index.

Sample	Sardinian sector	ρ_S (g/cm^3)	ρ_R (g/cm^3)	ρ_B (g/cm^3)	Φ_O He (%)	Φ_C He (%)	Φ_O H_2O (%)	Φ_C H_2O (%)	Φ_T (%)	IC_W (%)	SI (%)
CPZ1	Morgongiori	2.40	2.37	2.13	10.2	1.2	8.3	1.9	11.4	3.87	81.4
CPZ2a	Morgongiori	2.44	2.42	1.76	27.1	0.8	23.0	4.1	27.9	13.06	84.9
CPZ2b	Morgongiori	2.58	2.55	2.15	15.8	1.0	11.7	4.1	16.8	5.47	74.4
CPZ3a	Morgongiori	2.51	2.32	1.94	16.7	6.1	14.1	2.6	22.8	7.28	84.5
CPZ3b	Morgongiori	2.52	2.43	2.27	6.2	3.4	4.5	1.8	9.6	1.96	71.6
CPZ4	Morgongiori	2.49	2.35	2.01	14.6	4.8	12.0	2.6	19.3	5.97	82.6
CPZ5	Morgongiori	2.39	2.35	2.17	7.4	1.8	6.0	1.4	9.2	2.77	80.9
CPZ6	Morgongiori	2.57	2.53	2.22	12.2	1.2	10.8	1.4	13.4	4.87	88.7
CPZ7	Morgongiori	2.38	2.34	1.66	28.9	1.1	27.0	1.9	29.9	16.19	93.5
CPZ8	Morgongiori	2.40	2.37	2.09	11.7	1.0	9.1	2.6	12.7	4.35	77.7
CPZ9	Asuni	2.50	2.48	1.51	39.2	0.7	38.0	1.2	39.9	25.28	97.1
CPZ10	Ruinas	2.68	2.67	1.78	33.4	0.4	32.9	0.5	33.8	18.55	98.8
CPZ11a	Fordongianus	2.65	2.60	1.60	38.5	1.3	38.4	0.1	39.8	24.05	99.9
CPZ11b	Fordongianus	2.67	2.65	1.67	36.9	0.4	36.8	0.1	37.3	22.00	99.9
CPZ12	Serrenti	2.67	2.62	2.07	20.8	1.6	17.5	3.2	22.4	8.46	84.6
CPZ13a	Romana	2.31	2.28	1.41	38.0	0.8	37.8	0.3	38.8	26.74	99.5
CPZ13bS	Romana	2.40	2.29	1.42	38.1	2.7	36.4	1.7	40.8	25.65	95.7
CPZ13bA	Romana	2.32	2.28	1.47	35.4	1.0	35.2	0.2	36.4	23.85	99.7
CPZ14a	Romana	2.32	2.10	1.60	23.7	7.5	22.5	1.2	31.2	14.08	95.2
CPZ14b	Romana	2.33	2.21	1.59	28.0	3.5	26.4	1.6	31.5	16.58	94.5
CPZ15a	Osilo	2.88	2.88	1.98	31.1	0.1	29.3	1.8	31.1	14.77	94.4
CPZ15b	Osilo	2.78	2.64	2.28	13.4	4.5	11.8	1.6	17.9	5.17	88.1
CPZ17a	Osilo	2.72	2.60	2.03	22.2	3.5	20.5	1.7	25.6	10.11	92.5
CPZ18	Mores	2.40	2.38	1.87	21.4	0.7	17.8	3.6	22.1	9.51	83.3
CPZ20a	Monastir	2.63	2.54	2.03	20.1	2.6	16.9	3.2	22.7	8.33	84.4
CPZ20b	Monastir	2.78	2.78	2.40	13.6	0.1	10.7	2.9	13.7	4.46	78.9

the strength index is also present within individual groups of vulcanites from the same area.

Mechanical strength is highest in vulcanites showing low porosity and high bulk density (Table 5, Fig. 9; e.g., in the samples from Asuni, Ruinas and Fordongianus). Resistances are also low in the case of vulcanites with a high degree of alteration, as for example in most of the samples from Romana and some from Osilo (Fig. 9), and especially in samples from Morgongiori, which show very low values of the PLT strength index (< 3.8 MPa, Table 5).

4.2. *Pozzolanic reactivity test between volcanic rocks and hydrated lime*

The reactivity between ground vulcanites and hydrated lime was determined by means of the Chapelle test, as reported in Table 6. The most reactive samples (*i.e.,* those that bound the higher amount of $Ca(OH)_2$) were the perlitic samples from the Mt. Sparau (Morgongiori, Central-Western Sardinia) CPZ1: 687 mg/g; CPZ5: 744 mg/g; CPZ8: 687 mg/g; and the rhyolitic pyroclastite samples from the Fordongianus quarry CPZ11a: 730 mg/g; CPZ11b: 707 mg/g. Considered that, according to Jankovský et al. and references there in [69], a mineral admixture is considered pozzolanic as the minimum mass of $Ca(OH)_2$ consumed is 436 mg/g, the results indicate that these volcanic rocks can enhance pozzolanic properties (and thus hydraulicity) and mechanical strength in mortar production. The ubiquitous presence of glass in these vulcanites suggests that this could be the main factor influencing the reactivity between volcanic rocks and hydraulic lime. However, as shown in Table 3 and Figs. 3–6, glass is present in all samples, though with different fraction. Interestingly, some samples with lower glass content still exhibit good reactivity, suggesting that additional factors play an equally significant role in determining reactivity. The samples that did not show good reactivity (CPZ3b, 7, 10, 12, 13bS, 14b, 20b), with bound $Ca(OH)_2$ values always below 29 mg/g (Table 6), came from almost all the sampled areas in Sardinia, with the exception of the Fordongianus area.

4.3. *SEM analyses of the reactive pozzolans*

To better define the variables affecting the reactivity between the selected volcanic rocks and the hydrated lime (see next Section 4.4), the compositional, microstructural and textural characteristics of the three most reactive vulcanites (*i.e.*, CPZ1, CPZ5, CPZ11a) and one of the least reactive samples (CPZ13bS) were analysed in thin sections by scanning electron microscopy (SEM).

Perlitic sample CPZ1 exhibits a substantially glassy matrix (Fig. 10) with typical eutaxitic texture, and a silica-aluminous-(potassic) composition, low in Na, Ca, Fe, Mg. Alternating amorphous and crystalline bands are well developed; the porosity, generally low, is concentrated in pore-rich domains.

The glass shows subconcentric fractures (Fig. 10). Especially in the more crystalline bands, the presence of plagioclase, rarer K-feldspar and biotite is observed. The latter varies in size from small crystals (30–50 μm) embedded in the matrix to submillimetric

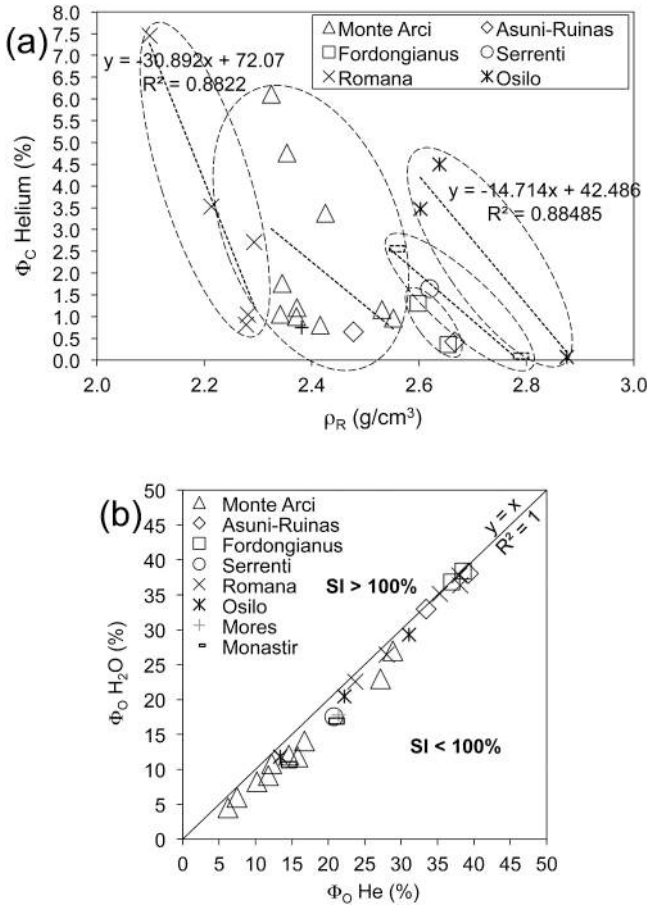

Fig. 8. Physical properties of Sardinian volcanics rocks sampled for this study: (a) real density vs. helium closed porosity; (b) helium open porosity vs. water open porosity.

phenocrysts. Non-silicates ("opaques") minerals (<1 %) are observed, typically dispersed in the matrix and sometimes located within the biotite. Additionally, quartz has been occasionally detected with a sub-rounded shape.

Sample CPZ5 has a mainly glassy matrix (>80 %vol.; Fig. 11) characterised by a Si-Al-Na-K composition with low Fe content. The crystalline fraction is represented by plagioclase (often as relicts), rare K-feldspar and biotite, which is sometimes found within feldspars. Quartz crystals, generally with a subrounded habit (Fig. 11), and Fe-Ti oxides ("opaque minerals", Fig. 10), are disseminated in the glassy matrix.

Sample CPZ11a shows a very porous, moderately welded microparticle matrix (Fig. 12), mainly consisting (about 80 %vol.) of both micrometric crystals immersed in the groundmass to submillimetre-sized phenocrysts of plagioclase, K-feldspar, biotite and rare pyroxene. Plagioclase phenocrysts, often hosting opaque minerals, show a variable composition, from albite to andesine (Fig. 12a). Opaque minerals consist of Fe and Fe-Ti oxides scattered in the matrix (approximately 3–4vol%). Apatite is also occasionally observed, often in contact with ilmenite (Fig. 12b). Occasionally, compact glassy plaques ranging from 700 to 1200 μm in size, have been observed, within which a higher concentration of opaque minerals (usually smaller than 50 μm in size) is present. The amorphous phase (< 20 %vol.) is represented by welded and elongated pumices, glassy juvenile and cognate fragments, occasional xenolithics. There are also millimetric co-magmatic hypocrystalline fragments, with a porphyritic microstructure for phenocrystals of plagioclase and pyroxene; the contact between the fragments and the rock matrix is marked by an interlayer (550 μm in thickness) characterised by secondary minerals (greenish under polarised optical microscopy), probably consisting of celadonite (Fig. 12c).(c)

The CPZ13bS sample, one of the least reactive with lime, is characterized by a hypocrystalline textures with glassy matrix < 30 % vol. (Figs. 3, 13), having Si-Al-Ca-K composition with a low concentration of sodium and very low iron and magnesium content. In the sample, the crystalline components, consisting of phenocrysts and microliths embedded in the groundmass, include plagioclase, biotite, and opaque minerals, such as Ti-magnetite and ilmenite (Fig. 13); occasional zircon crystals have also been found. The matrix contains irregular microcracks and cavities (Fig. 13), with diameters ranging from sub-micrometric (<5 μm, Fig. 13c) to sub-millimetric. Microliths of zeolites (mainly clinoptilolite, Table 3) are arranged in a radial pattern near the cavity walls, and appear felt-like in the central part (Fig. 13c). Among these, microcrystals of feldspar and clay minerals are occasionally observed (Fig. 13c).

Table 5
Physical-mechanical properties of the volcanic rocks as obtained by the Point Load Test (PLT).

Sample	Load (N)	2 L (mm)	W (mm)	H (mm)	De^2 (mm^2)	De (mm)	Is (N/mm^2)	F /	$Is_{(50)}$ (MPa)
CPZ1	300	18.6	17.2	17.2	371.9	19.3	0.8	0.7	1.2
CPZ2a	1700	17.4	15.5	15.5	295.6	17.2	5.8	0.6	9.3
CPZ2b	1300	10.6	7.9	8	72.7	8.5	17.9	0.5	39.7
CPZ3a	1350	15.3	14	14	240.2	15.5	5.6	0.6	9.5
CPZ4	1100	16.4	12.6	12.7	192.5	13.9	5.7	0.6	10.2
CPZ5	250	18.3	16.3	16.2	320.7	17.9	0.8	0.6	1.2
CPZ6	2450	15.6	13.9	13.9	230.1	15.2	10.6	0.6	18.2
CPZ7	950	12.5	11.1	11.1	148.1	12.2	6.4	0.5	12.1
CPZ8	650	17.9	15.3	15	279.2	16.7	2.3	0.6	3.8
CPZ9	1800	15.7	11.8	11.9	173.1	13.2	10.4	0.5	19
CPZ10	500	17.4	15.4	15.3	282.5	16.8	1.8	0.6	2.9
CPZ11a	450	13.7	10.7	10.9	144.1	12	3.1	0.5	5.9
CPZ11b	650	16.3	15.7	15.8	296.3	17.2	2.2	0.6	3.5
CPZ12	2250	13.9	12.7	12.6	184.9	13.6	12.2	0.6	21.9
CPZ13a	100	20.3	18.8	18.8	430.3	20.7	0.2	0.7	0.3
CPZ13bS	350	18.7	17.5	17.6	379.9	19.5	0.9	0.7	1.4
CPZ13bA	400	16.4	14	14.1	250.5	15.8	1.6	0.6	2.7
CPZ14a	2700	17.3	15.3	15.3	291.7	17.1	9.3	0.6	15
CPZ14b	1100	15.6	12.9	12.8	204.5	14.3	5.4	0.6	9.4
CPZ15a	2500	17.4	16.2	16	317.3	17.8	7.9	0.6	12.5
CPZ15b	2000	18.1	15.6	15.7	308.4	17.6	6.5	0.6	10.4
CPZ17a	550	15.3	12.5	12.6	191.4	13.8	2.9	0.6	5.1
CPZ18	1700	18.3	16.2	16.3	330.5	18.2	5.1	0.6	8.1
CPZ20a	1800	18.6	17.2	17.1	359.8	19	5	0.6	7.7
CPZ20b	4550	16.8	14.4	14.5	257.6	16	17.7	0.6	29.5

4.4. Thermogravimetric analyses (TGA, DTG) of the reactive pozzolans

TGA analyses were performed on six samples, selecting the three most reactive lithologies with lime (see results of Chapelle test in Table 6), CPZ1, CPZ5, CPZ11, as well as the three least reactive, namely CPZ10, CPZ13bS and CPZ14b. Fig. 14 reports, for each sample, the TG curve (solid line) and the DTG curve (dashed line). Significantly different trends, among the analysed samples, can be observed. The least reactive samples, CPZ13bS and CPZ14b, show similar TG curves with relative weight loss higher if compared to the other samples. The high weight loss of CPZ13bS and CPZ14b is mainly due to the zeolite content, as suggested by XRD analyses (about 54 % and 40 % of clinoptilolite, respectively; Table 3), and by the shape of the TG curves, similar to those reported in literature for clinoptilolites [70–72]. Both samples show a continuous and intense weight loss from the beginning of the heating ramp (25 °C) to approximately 200 °C, resulting in a steep TG curve. Above approximately 200 °C, the weight loss slows but continues until reaching a plateau at 600–650 °C. DTG curves (Fig. 14) shows a marked inflexion below 100 °C, likely related to the loss of hygroscopic water, followed by loosely bonded H_2O molecules up to 200 °C, and finally by the loss of strongly bonded molecules at higher temperature [70,73,74].

The samples CPZ1 and CPZ5, two of the most reactive samples, share similar TG curves consisting of a single loss event ranging from about 200–400 °C with a maximum rate at about 300 °C, and a total loss lower than 2 %. In this case, the weight loss is primarily attributed to the volcanic glass, which represents over 80 % in both samples. This is supported by literature data indicating a similar temperature range for rhyolitic volcanic glasses [75]. The TG curves of samples CPZ10 and CPZ11a exhibit distinct behaviours. CPZ11a, one of the most reactive samples, shows a total weight loss of less than 0.5 %, primarily within the first 100 °C of the heating ramp, likely due to sample humidity. This minimal weight loss is consistent with its low glass content (13 %) and the absence of zeolites or other hydrous minerals. In contrast, CPZ10 loses weight from the beginning of the heating ramp up to approximately 600 °C. Beyond this point, the weight loss rate increases, as shown by an endothermic peak at 625 °C in the DTG curve. Above 650 °C, the loss continues with a rate similar to that observed in the first part of the curve, reaching a total loss of about 2.2 % at the end of the test. The thermal behaviour of CPZ10, selected as one of the less reactive, is difficult to explain; XRD analysis indicates low contents of glass (7 %) and zeolite (laumontite, 1.2 %) and the absence of other minerals that could produce a weight loss in the 600–650 °C range.

Notably, the most reactive samples (CPZ1, CPZ5, and CPZ11a) exhibit the lowest total weight loss, ranging from 0.5 wt% (CPZ11a) to 2 wt% (CPZ1 and CPZ5; Fig. 14). The highly glassy perlitic samples CPZ1 and CPZ5, containing 81 % and 86 % glass, respectively (Table 3), lose weight primarily between 200 °C and 400 °C, corresponding to dehydration and dehydroxylation processes. In contrast, CPZ11a, with a much lower glass content (23 %, Table 3) and minimal weight loss, displays a constant rate of weight loss throughout the heating ramp, without any observable endothermic peak (Fig. 14).

4.5. Mineralogical and petrographic features of pozzolanic mortars

The pozzolanic mortar, observed under polarized light microscopy in thin sections, show a homogeneous micritic binder in which the aggregates, both pozzolans and sand minerals, are clearly recognizable. The photomicrographs of the mortar (Fig. 16) also reveal

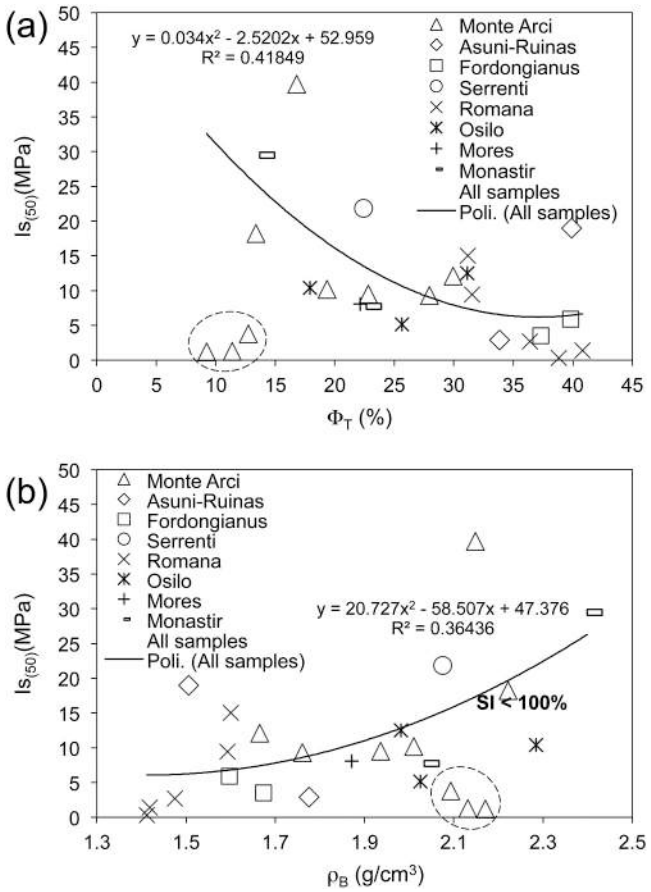

Fig. 9. Physical-mechanical properties of the volcanic rocks: (a) total porosity vs. point load strength index $Is_{(50)}$; (b) bulk density vs. point load strength index $Is_{(50)}$.

reaction rims between the pozzolanic fragments and the lime binder, highlighted by higher birefringence compared to the surrounding binder.

The very fine grain size of the binder prevents the optical identification of its mineral's constituents. However, XRD analyses conducted on aged mortars (up to two years), indicate that the binder contains calcite, which forms as a result of the carbonation process (Fig. 15), and portlandite [$Ca(OH)_2$], deriving from the slaked lime binder ("grassello", indicating a not completed carbonation. The presence of hydraulic phases (C-S-H or C-A-H) cannot be confirmed through optical or XRD, as the analysis does not reveal peaks corresponding to these phases.

Although all selected pozzolans underwent the same preliminary physical treatment to achieve a uniform grain size before being used as aggregate in the mortars, they exhibit different degrees of angularity and rounding, depending on their petrogenesis. Volcanic rocks with greater compactness and mechanical strength tend to be more angular, whereas those with lower internal cohesion —typically the more reactive ones, such as pyroclastic CPZ11a and perlitic facies CPZ1, CPZ5, and CPZ8— show a higher degree of roundness. These differences are evident in both optical microscopy and SEM images (Figs. 16 and 17).SEM analyses of the selected mortars made up with sand aggregate, slaked lime binder and the more reactive pozzolans (CPZ5 and CPZ11a samples; Fig. 17) at curing 1 year, show the presence of low fraction of C-S-H phases (Fg. 17a). Analytical data from the inner surface (see spectrum in Fig. 17b) of the cavity suggest a composition similar to that of a C-S-H phase. The CPZ11a sample, used as a pozzolan in the mortar, demonstrates a strong reaction with the lime binder (Fig. 17c). The spectrum in Fig. 17d indicates a composition similar to the C-S-H phase, although the Si concentration exceeds the expected stoichiometric ratio. Additionally, the spectrum in Fig. 17f corresponds to a plagioclase crystal (Fig. 17e), but with high content of Ca and C, likely attributable to a calcite patina coating the plagioclase.

4.6. Physical-mechanical tests on pozzolanic mortars

Tables 7 and 8 show the results of the mechanical tests (compressive and flexural) performed on the mortar specimens made by hydrated lime, standardized Qz-rich sandy aggregate, pozzolan and water. The four samples of vulcanites selected as pozzolan (*i.e.,* CPZ 11a, 13a, 13bS, 14b) for the mortars were selected based on their varying reactivity as determined by the Chapelle test: high

Table 6
Results of Chapelle chemical reactivity test between the selected powered volcanic rocks and slaked lime.

Data test				Reagent			Titration		Results		
Sample	Amount material (mg)	*T* (°C)	Time (h)	Ca $(OH)_2$ (mg)	CaO free (%)	CaO avail. (mg)	HCl (mg)	Correction coef. HCl	$Ca(OH)_2$ residual (mg)	$Ca(OH)_2$ bound (mg)	CaO bound/ avail. (wt%)
CPZ 1	1000.1	90	16	1276.2	66.7	851.2	11.1	1	411.1	713.2	63.4
CPZ2a	1001.0	90	16	1275.0	66.7	850.4	18.3	1	677.8	445.1	39.6
CPZ2b	1000.8	90	16	1277.0	66.7	851.8	19.5	1	723.0	401.8	35.7
CPZ3a	1000.2	90	16	1272.3	66.7	848.6	15.9	1	588.9	532	47.5
CPZ3b	1000.2	90	16	1280.0	66.7	853.8	22.4	1	829.7	298	26.4
CPZ4	1000.9	90	16	1273.9	66.7	849.7	19.9	1	737.1	385	34.3
CPZ5	1000.8	90	16	1274.0	66.7	849.8	10.2	1	377.8	744.1	66.3
CPZ6	1000.8	90	16	1277.0	66.7	851.8	15.5	1	574.1	550.6	48.9
CPZ7	2000.8	90	17	2277.0	67.7	1541.5	16.5	2	1222.3	406.8	20.0
CPZ8	1001.0	90	16	1272.9	66.7	849.0	11.7	1	433.4	687.5	61.3
CPZ9	1001.0	90	16	1277.0	66.7	851.8	20.5	1	759.3	365.5	32.5
CPZ 10	1000.0	90	16	1278.2	66.7	852.6	25.8	1	955.6	170.6	15.1
CPZ11a	1000.8	90	16	1271.0	66.7	847.8	10.5	1	388.9	730.4	65.2
CPZ11b	1000.2	90	16	1276.0	66.7	851.1	11.3	1	417.1	707.1	62.9
CPZ 12	1000.8	90	16	1279.5	66.7	853.4	24.0	1	889	238.2	21.1
CPZ13a	1001.0	90	16	1275.0	66.7	850.4	18.5	1	685.2	437.7	39.0
CPZ13bS	1000.8	90	16	1276.0	66.7	851.1	25.4	1	940.8	183.3	16.3
CPZ13bA	1000.8	90	16	1272.0	66.7	848.4	15.2	1	563	557.3	49.7
CPZ14a	1000.2	90	16	1276.0	66.7	851.1	17.4	1	643	481.2	42.8
CPZ14b	1001.0	90	16	1277.0	66.7	848.0	25.6	1	948.2	176.7	15.7
CPZ15a	1000.8	90	16	1275.0	66.7	856.0	18.6	1	687.5	435.6	38.8
CPZ15b	1000.0	90	16	1273.0	66.7	849.0	17.5	1	648.2	473.4	42.2
CPZ17a	1000.0	90	16	1274.0	66.7	857.0	15.6	1	577.8	544.7	48.5
CPZ18	1000.0	90	16	1271.0	66.7	850.0	16.3	1	603.8	516.1	46.1
CPZ19	1001.0	90	16	1272.0	66.7	845.0	18.5	1	685.2	435.1	38.8
CPZ20a	1000.8	90	16	1275.0	66.7	862.0	19.5	1	722.3	400.8	35.7
CPZ20b	1000.9	90	16	1275.0	66.7	854.0	21.5	1	796.4	326.7	29.1

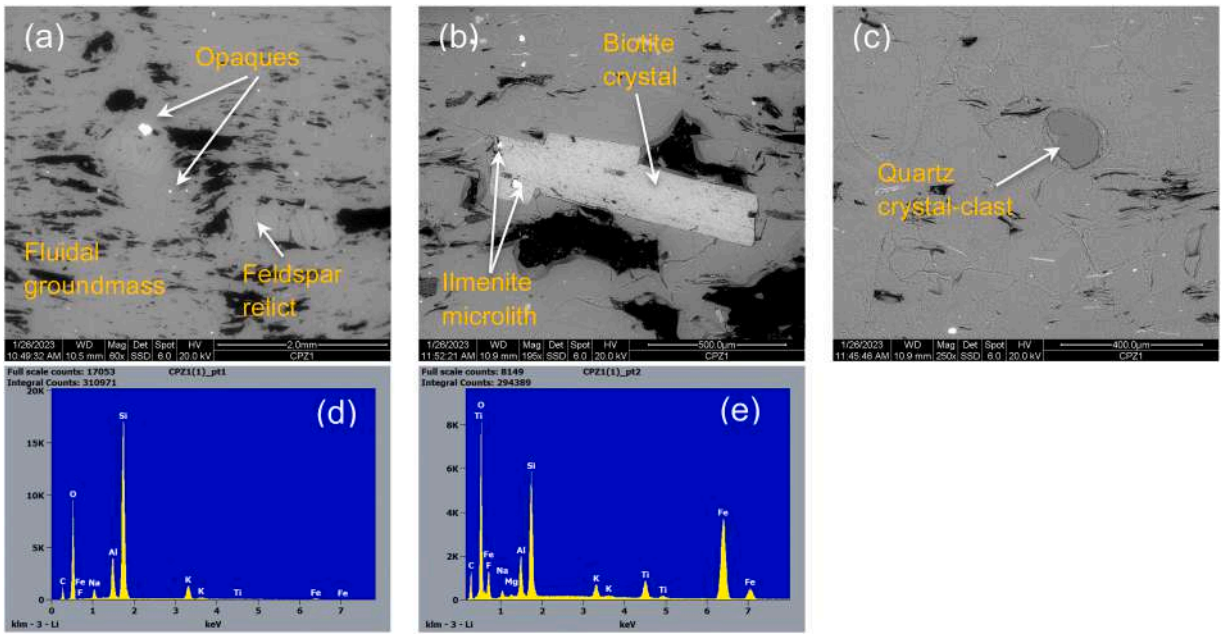

Fig. 10. SEM images of rhyolitic pyroclastic rocks CPZ1 from Mt. Sparau quarry. (a) Sample characterized by a high porous glassy microstructure with fluidal texture and dissemination of opaque minerals and a fractured feldspar relict (BSE); (b) ilmenite microcrystals within a biotite crystal (BSE); (c) quartz crystal-clast with concentric fracturing structures within the glassy groundmass (BSE); SEM-EDS spectrums of Fe-oxide (d) and of the glassy matrix (e).

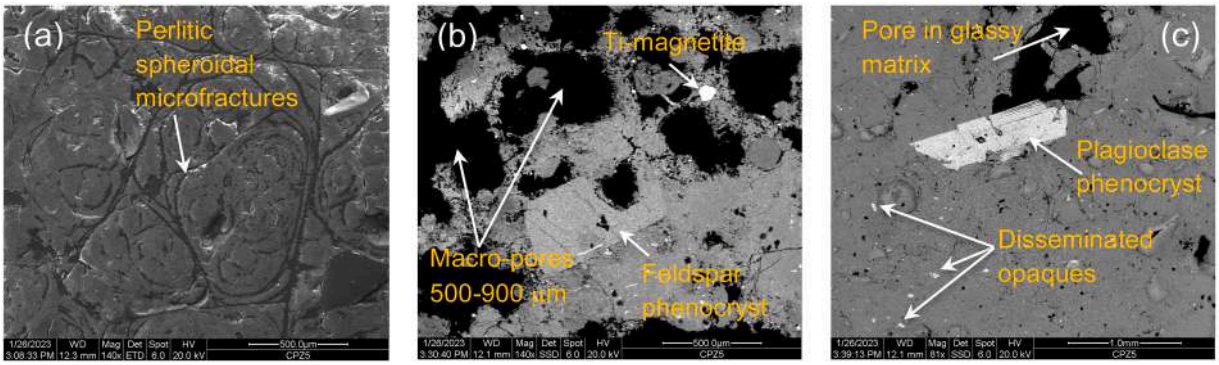

Fig. 11. SEM images of rhyolitic pyroclastic rocks CPZ5 from Mt. Arci quarry. (a) Porous hypoialine groundmass with perlitic microstructure, spheroidal microfractures (SE); (b) rare crystalline component, mainly represented by feldspar and disseminated opaque minerals (Ti-magnetite) (BSE); (c) plagioclase phenocrystals and opaques immersed in the glassy matrix (BSE).

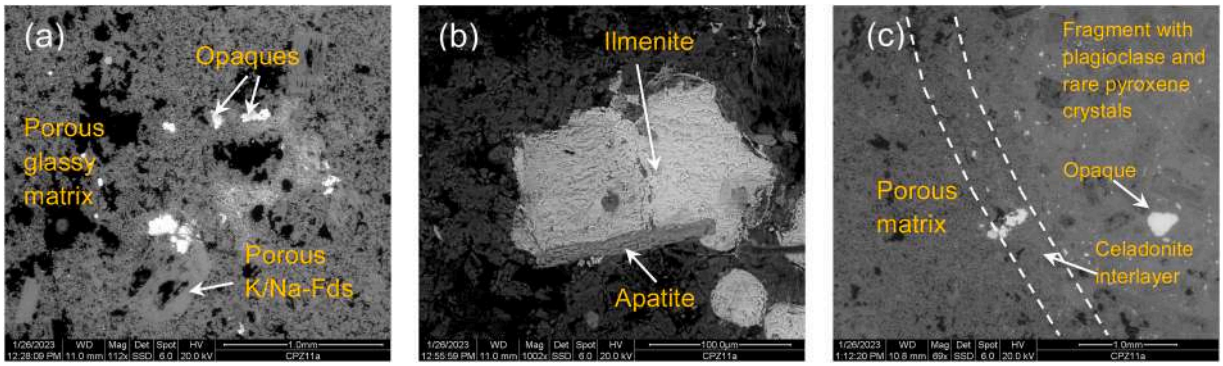

Fig. 12. SEM images of rhyolitic pyroclastic rocks CPZ11a from Fordongianus quarry. (a) Porous glassy microstructure with dissemination of opaque minerals and porous K/Na-feldspar relict (BSE); (b) ilmenite crystal with associated apatite crystal (BSE); (c) juvenile/cognate fragment (right side of imagine) with plagioclase microliths within the glassy porous matrix of rock (left side) (BSE).

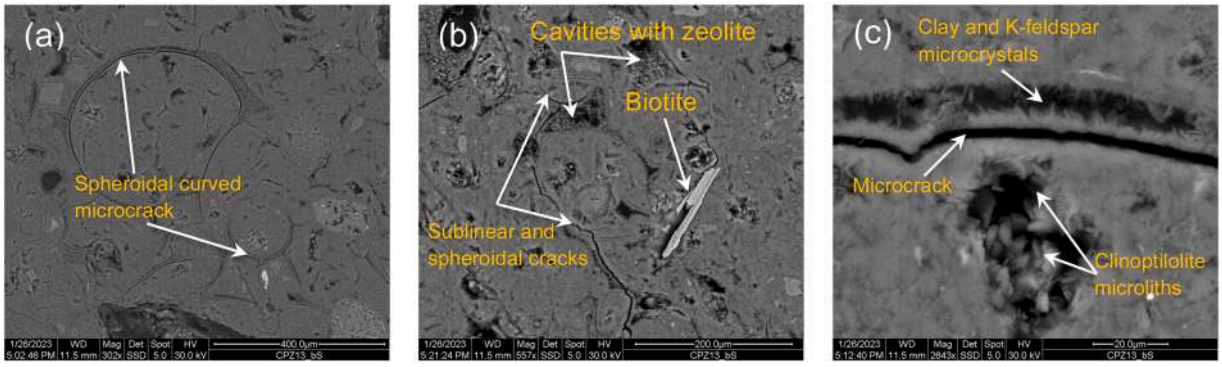

Fig. 13. SEM images of rhyolitic pyroclastic rocks CPZ13bS from the Romana area. (a) Spheroidal curved microcracks within the not very glassy microstructure (BSE); (b) from hypoialine to hypocrystalline groundmass with biotite crystal and disseminated zeolite microliths (elongated up to 8–10 μm) within the microcavities (generally with size < 100 μm (BSE); (c) detail of microstructure with radial clinoptilolite microcrystals within the microcavities, and clay and K-feldspar microliths (suborthogonal to the wall) inside elongated pores subparallel to the microcracks (BSE).

reactivity (*i.e.,* CPZ 11a), to intermediate reactivity (*i.e.,* CPZ 13a), and low reactivity (*i.e.,* CPZ 13bS, 14b). The mechanical tests show good performance for the mortars in which vulcanite of rhyodacitic-riolitic samples (*i.e.,* sample CPZ 11a, from the Fordongianus quarry) were used. This vulcanite shows values of 730.4 mg $Ca(OH)_2$ bound and 65 % CaO bound/available ratio (Table 6). Compressive strength values ranging from 8.63 to 13.2 MPa were obtained 20 days after mortar preparation, with an increase by double (*i.e.,* 15.2–16.2 MPa) after 30 days (Table 7). Sample CPZ13a, sourced from the NorthEast Romana area, exhibited 437.7 mg of

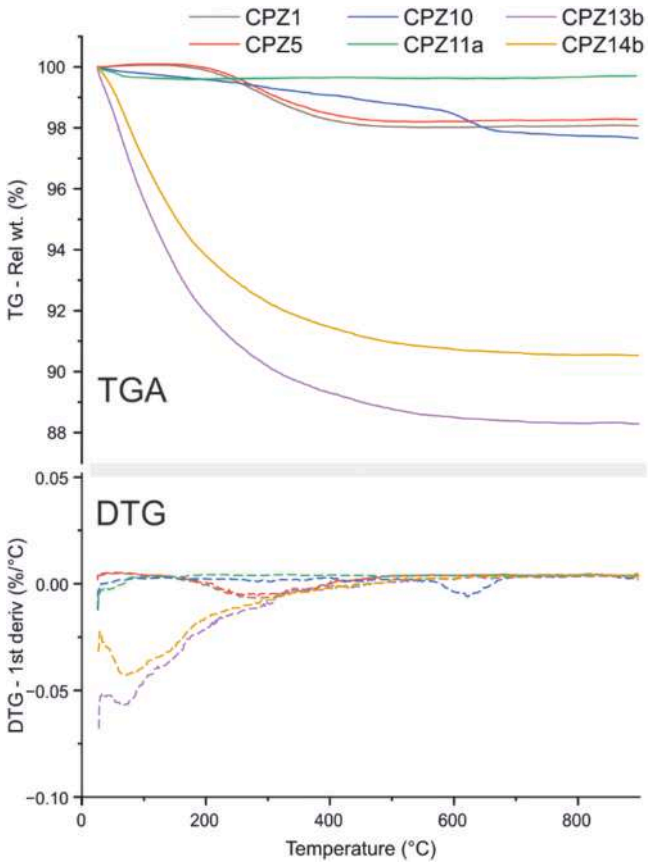

Fig. 14. TG and DTG curves of most reactive (CPZ1, 5, 11a) and less reactive pozzolans (CPZ10, 13b, 14b).

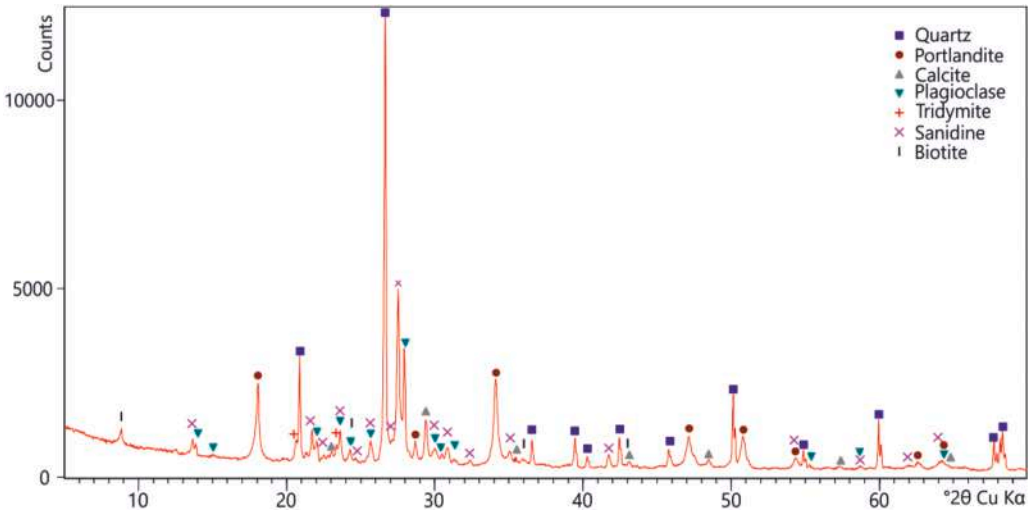

Fig. 15. XRD diffraction pattern of a selected powered pozzolanic mortar made up with volcanic rocks, sand aggregate and slaked lime binder.

bound $Ca(OH)_2$ and a 39 % CaO bound/available ratio (Table 6).

Despite these values, it showed considerably lower compressive strength if compared to the sample CPZ11a. The compressive strength of CPZ13a ranges between 7.89 and 8.35 MPa after 20 days and increases to 12.79–13.85 MPa after 30 days (Table 7). In contrast, sample CPZ13bS, also from Romana, demonstrated lower reactivity with 183.3 mg of bound $Ca(OH)_2$ and a 16.3 % CaO bound/available ratio (Table 6), resulting in strength values that did not exceed 0.75 MPa, even after 30 days (Table 7).

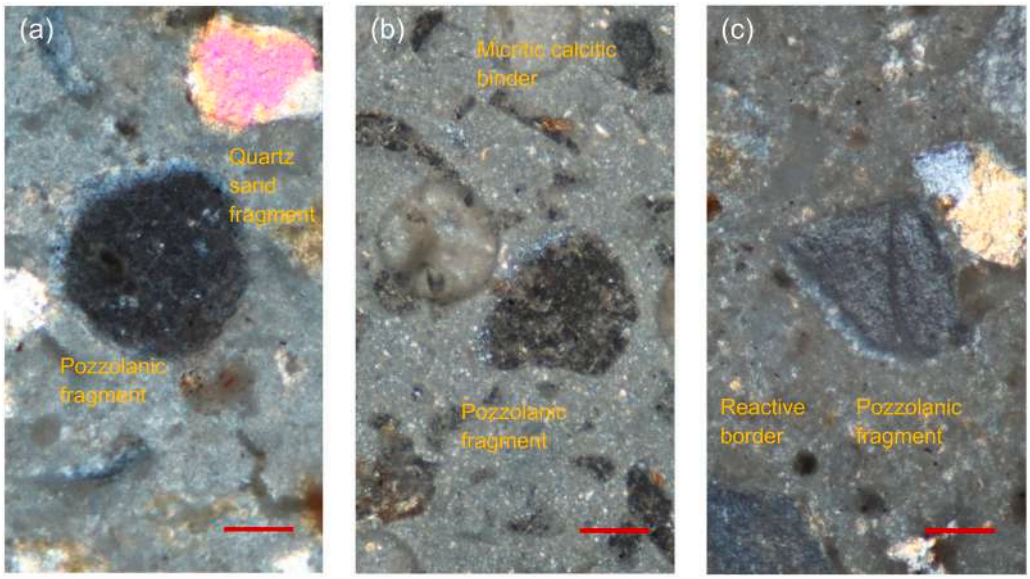

Fig. 16. Thin-section microphotographs of the selected pozzolanic mortars at 1 year curing time made by reactive volcanic rocks, sand aggregate and slaked lime binder. (a) CPZ1 pozzolanic fragment within a micritic binder; (b) CPZ5 pozzolan fragment within a micritic binder; (c) CPZ11a pozzolan fragment within a micritic binder. Red bar = 150 μm.

The flexural tests show, although to a lesser extent, a similar physical-mechanical behaviour of the four selected samples to that of compression (Table 8). Vulcanite from Fordongianus (*i.e.,* sample CPZ11a) has strength values between 2.92 and 2.99 MPa, while sample CPZ13a ranges between 2.56 and 2.89 MPa. On samples CPZ14b and 13bS, no significant values could be determined due to their low strength.

5. Discussion of results

In this paper, the chemical reactivity between lime and the volcanic rocks from different outcrops of Sardinia (*i.e.*, Morgongiori, Asuni, Ruinas, Fordongianus, Serrenti, Romana, Osilo, Mores and Monastir) was studied, in order to assess their use as pozzolan in the production of hydraulic mortars with low environmental impact.

The mineralogical and petrographic analysis highlighted that the volcanic rocks here studied have a composition from basic-intermediate to acidic (from andesitic, to dacitic, to rhyolitic) and are characterized by the variable weight fraction of glass (from 5 % to 99 %) and, locally, zeolites and other secondary minerals (*e.g.*, phyllosilicates).

The studied samples exhibited properties (*e.g.*, density, porosity, water absorption, mechanical resistance, etc.) primarily influenced by differences in the mineralogical composition, textures and microstructures. These variations were further linked to the type and fraction of glass *vs.* crystalline species, their distinct modes of emplacement (determined by temperature, chemical composition, and degree of welding), as well as the extent of chemical and mineralogical alteration. Based on the results, volcanic rocks, with basic or intermediate compositions, generally exhibit lower open porosity to helium, with values ranging from 13.6 % (*i.e.*, Monastir andesites) to 20.8 % (*i.e.*, Serrenti dacites). The typical pyroclastic rocks (with a composition ranging from rhyodacitic to rhyolitic) from Fordongianus, Ruinas, Asuni, Romana, Mores, show higher porosity, ranging from 21.4 % (*i.e.*, Mores volcanics) to 39.2 % (*i.e.*, Asuni rhyolites), due to the different compositional incidence of abundant pumices, shards, phenocrysts, groundmass microlithics, cognate fragments, xenoliths. The rhyolitic perlites from Monte Arci (Morgongiori) and the vulcanites from Osilo show very variable values. The formers have a porosity ranging from 6.2 % (*i.e.*, sample CPZ3b) to 28.9 % (*i.e.*, sample CPZ7); considering that both samples have a very high fraction of glass (respectively: 99 and 97 %, Table 3), such differences in porosity are attributable to the different conditions of the vulcanites emplacement, which have led to different conformations of the concentric and linear micro-cracking and welding degree. For example, the CPZ4 sample is characterized by a compact perlitic microstructure, while the CPZ7 sample shows a diffusely porous microstructure, partly due to the presence of blackish iso-oriented shards (Table 2). The Osilo vulcanites show porosities ranging from 13.4 % (*i.e.*, sample CPZ15b) to 31.1 % (*i.e.*, sample CPZ 15a), mostly due to epigenetic processes that have led to different degrees of alteration and recrystallization phenomena, even within the same sample. Due to the high helium-open porosity of the pyroclastics, the most porous samples (*i.e.*, Asuni, Ruinas, Fordongianus, Romana) are those that also have high water absorption values with imbibition coefficients between 14.1 % and 26.7 %.

The bulk density ranges from a minimum of 2.1 g/cm^3 in the Romana pyroclastic rocks to 2.78 g/cm^3 in the Monastir sample, to 2.88 g/cm^3 in the high crystallinity sample from Osilo. This variation generally follows an inverse correlation with porosity, as shown in Fig. 7a. The bulk density ranges from a minimum of 2.1 g/cm^3 in the Romana pyroclastic rocks to 2.78 g/cm^3 in the Monastir sample, and up to 2.88 g/cm^3 in the high-crystallinity sample from Osilo. This variation generally follows an inverse correlation with

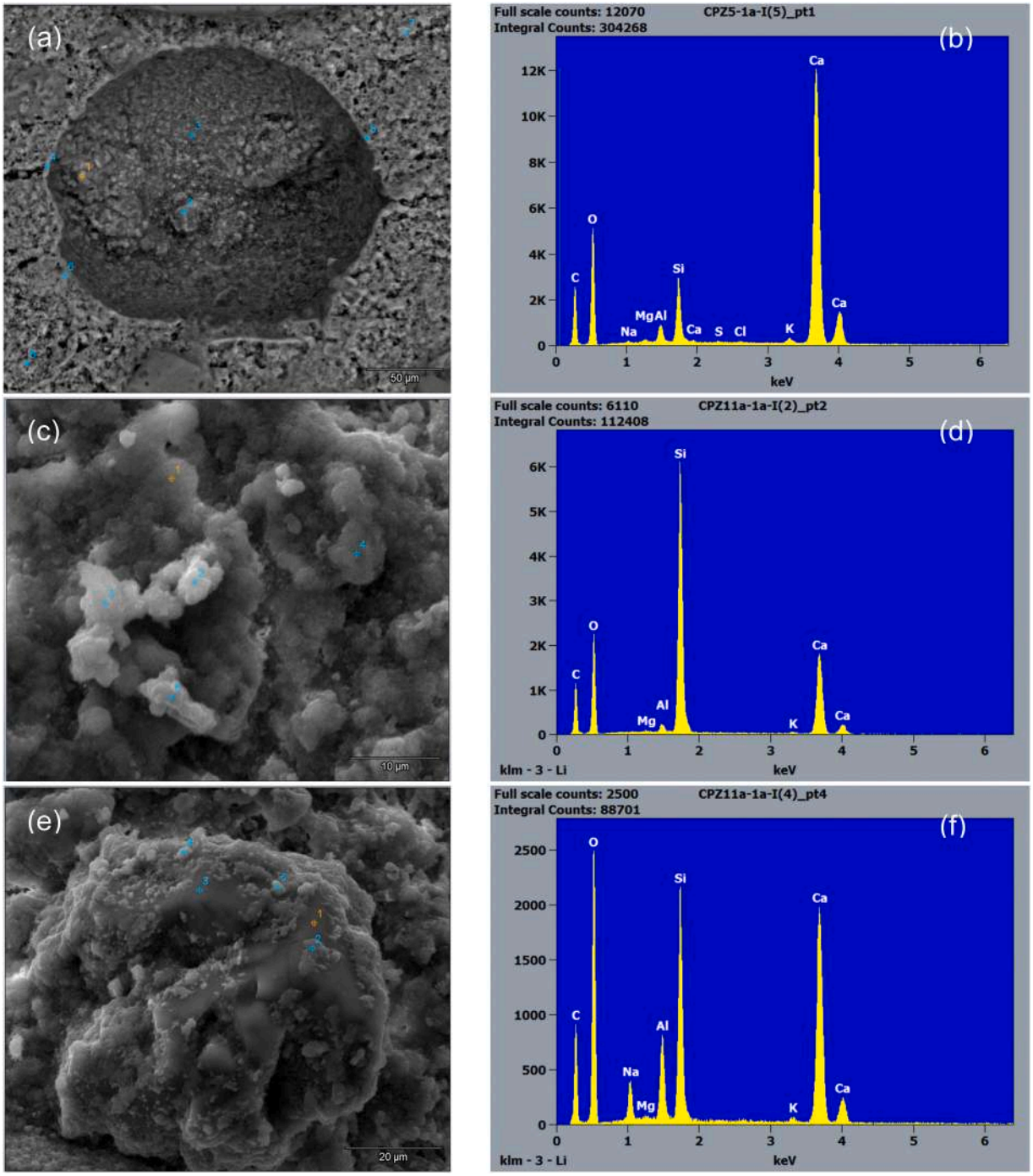

Fig. 17. SEM images of the main reactive pozzolanic mortars after one year of curing, made by reactive volcanic rocks CPZ5, 11a, sand aggregate and slaked lime binder. (a, b) CPZ5 pozzolanic mortar: void of a pozzolanic fragment; analytical data suggest a composition consistent with a possible C-S-H phase; (c, d) CPZ11a pozzolanic mortar: possible presence of C-S-H/C-A-H phases; (e, f) CPZ11a pozzolanic mortar: plagioclase crystal likely covered by a calcite patina resulting from Ca-carbonation.

porosity, as shown in Fig. 7. However, the bulk density is negatively correlated with the glass/crystallinity ratio and with the density of the solid phases (ρ_S; Fig. 7b), which in the case of the most basic samples (*i.e.*, andesites and partly in the dacites) is positively influenced by the higher fraction of the ferro-magnesian (mafic) phases with higher solid densities (3.40–4.79 g/cm^3), if compared to the sialic phases (2.53–2.65 g/cm^3).

The results of the reactivity tests (through the Chapelle method) highlighted that the best reacting vulcanites belong to the perlites

Table 7
Results of mechanical uniaxial compression (R_C) test of the mortars made by pozzolans CPZ11a, CPZ13a, CPZ 13bS and CPZ14b.

Sample	Specimen Ref.	(mm)	Specimen size (mm)	(mm)	R_C at 20 days (MPa)	R_C at 30 days (MPa)
CPZ11a	a	40	40	80	8.69	15.50
	b	40	40	80	8.63	15.20
	c	40	40	80	13.20	16.21
CPZ13a	a	40	40	80	7.89	12.79
	b	40	40	80	8.20	12.85
	c	40	40	80	8.35	13.85
CPZ13bS	a	40	40	80	0.17	0.52
	b	40	40	80	0.17	0.60
	c	40	40	80	0.18	0.75
CPZ14b	a	40	40	80	0.31	1.25
	b	40	40	80	0.45	1.21
	c	40	40	80	0.39	1.19

Table 8
Results of mechanical flexural test of the mortars made by pozzolans CPZ11a, CPZ13a, CPZ 13bS and CPZ14b. Abbreviations: n.d. = not determined.

Sample	Specimen Ref.	(mm)	Specimen size (mm)	(mm)	R_f at 20 days (MPa)
CPZ11a	a	40	40	160	2.92
	b	40	40	160	2.99
	c	40	40	160	2.94
CPZ13a	a	40	40	160	2.56
	b	40	40	160	2.89
	c	40	40	160	2.78
CPZ13bS	a	40	40	160	n.d.
	b	40	40	160	n.d.
	c	40	40	160	n.d.
CPZ14b	a	40	40	160	n.d.
	b	40	40	160	n.d.
	c	40	40	160	n.d.

sampled in quarry from Monte Arci (*i.e.*, samples CPZ1, 5, 8 from Morgongiori) and to the pyroclastics from the quarry of Fordongianus (*i.e.*, samples CPZ11a, 11b). Considering that the first three samples of Monte Arci all have a high fraction of glass (*i.e.*, 81, 86, 99 %, respectively), in these samples, if compared to the other less reactive ones, the glassiness parameter has positively influenced the chemical reactivity between pozzolan and hydrated lime (Fig. 18a). However, even though they have a similar chemical composition, different petrographic features are highlighted among the perlites, characterised by diverse distribution of crystallinity (between phenocrysts and groundmass) and glassy matrix. More precisely, samples CPZ1 and CPZ5, less glassy but more reactive than CPZ8, show a porphyritic structure with an index of 2–5 % and a hypohyaline groundmass (occasionally hyaline, Fig. 3e), while sample CPZ8 has a lower porphyritic index (<2 %) but a substantially hypohyaline groundmass, characterized by partial local microcrystallinity (Fig. 3h).

Conversely, the two Fordongianus samples (*i.e.*, CPZ11a, 11b) correspond to very similar facies with the same paragenesis, differing only in matrix colour and a slightly higher degree of alteration, and have a chemical composition comparable to that of the perlites, with a low glass content (5–13 wt%; Table 3). Despite this, the samples exhibit high reactivity (Table 6), nearly matching the most reactive sample, *i.e.*, CPZ5. Thus, in this case, the reactivity appears to be clearly influenced by factors other than the glass content. Observing the microstructural features of these pyroclastics at SEM, it can be observed that, unlike the perlitic facies, CPZ 11a, 11b have a fine porous groundmass with pore size mainly < 10 μm. Considering the sub-micrometric size of the pores, and that the pozzolan ground used in the Chapelle test had a grain size > 50 μm, the specific surface area of the CPZ11a sample, which remains high even after mechanical treatment, is pronouncedly higher than that of the perlitic CPZ1, 5, 8 samples. Therefore, the higher reaction surface area with the lime of the CPZ11a pozzolan quantitatively allows a higher reactivity with the lime, if compared to the perlitic CPZ1, 5, 8 samples. However, the latter have a higher specific chemical reactivity in the pozzolan-lime interface, as they are substantially amorphous materials.

Another factor that may have influenced the reactivity of pozzolans with lime is represented by the degree of hydration of the amorphous matrix. The glass in the reactive perlites from Mt. Arci (Morgongiori), which makes up over 81 % of the material, is generally more hydrated than the non-hydrated / non-perlitic obsidian facies [76]. This glass is more reactive than the glassy matrix of the pyroclastics of Fordongianus, which also exhibit an excellent reactivity with lime. This is partly also well highlighted by the L.O.I. wt% and by the TGA analysis (Fig. 14), which shows a general negative correlation with the reactivity. In fact, the most reactive samples (the Monte Arci perlites: CPZ1, CPZ5, and the Fordongianus pyroclastics: CPZ11a) have values lower than 2 % (Fig. 14), while the least reactive samples (CPZ13b, CPZ14b), show the highest L.O.I. values (about 9.2 % and 12.8 %, respectively, Fig. 14). Considering that the L.O.I. is generally positively correlated with the syn-epigenetic alteration, this indirectly highlights that the most

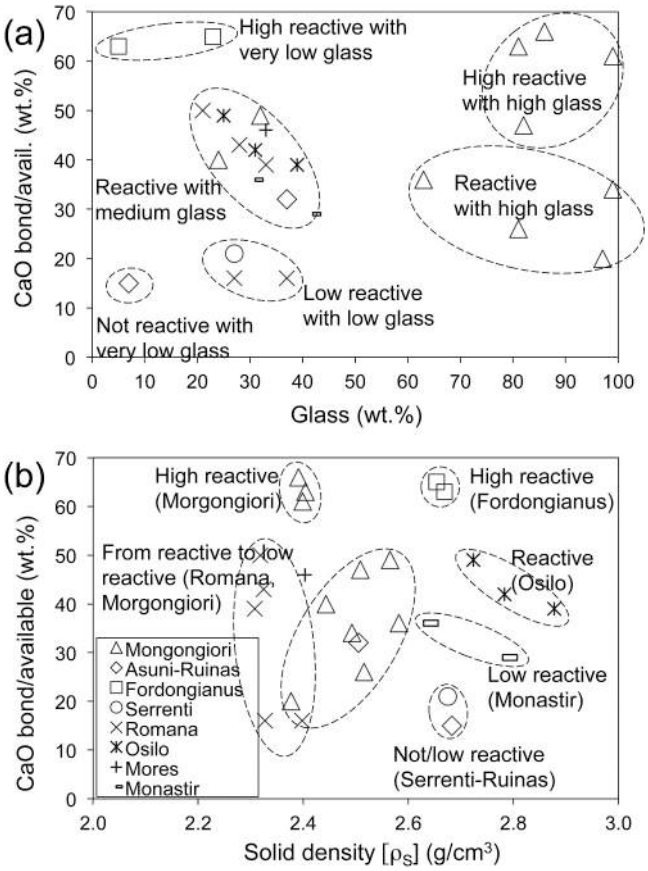

Fig. 18. (a) glass (wt.%) vs. CaO bond/avalilable; (b) solid density vs. CaO bond/avalilable.

reactive pozzolans are not (or little) altered. In support of this, the samples that did not react well with lime, in addition to having a low glass/crystallinity ratio, show not only magmatic mineralogy (*i.e.*, made by plagioclase, K-feldspar, pyroxene, quartz, occasional biotite) but also alteration mineralogy (secondary, by devitrification) in which zeolites, phyllosilicates (some also clay minerals), and carbonates (such as dolomite and calcite) occur (Table 3). Therefore, the crystallinity and mineralogical composition (strictly correlated to the density of the solid phases) influence the chemical reactivity in a non-obvious relation (Fig. 18b). The most zeolitized samples have low or poor reactivity with lime, highlighting that alteration may have deactivated the chemical reaction capacities. A comparison between the incidence of zeolite, especially when it occurs in very high concentrations (40–70 wt%: CPZ13, 14; Table 3), and the reactivity values shows a negative correlation. In support to this, the samples CPZ3 (perlite) and CPZ10 (pumiceous-cineritic pyroclastic), in force of their alteration (although modest, with the presence of zeolitic phases, Table 3), show a low reactivity. However, it is well known that zeolites, if present in moderate content in the mortar mix, can confer an improvement in the pozzolan-lime reaction, especially between 28 and 90 days of curing [77 and references there in] because the zeolite destabilization contributes Al and Si to the system resulting in C-A-S-H hydration products.

The physical- mechanical tests were critical to assess the reactivity of the studied vulcanites. The mortars were prepared using a highly reactive pozzolan from Fordongianus (Table 6, see CPZ11a) and three additional pozzolans with varying reactivity from the Romana area. The solid fraction of the mortar consisted of 5 % pozzolan, 9–10 % lime putty as a binder, an 85 % standardized quartz-feldspathic sand (grain size 0.08÷2 mm, according to UNI EN 196–1) as the aggregate; water slightly in excess of the required stoichiometric quantity was used to hydrate the mixture. The results of the mechanical compression and flexural tests performed on the specimens indicate that the mortars in which the rhyolitic composition CPZ11a pyroclastic material was used, gave good physical-mechanical performance, with compressive strength values 20 days after packaging ranging between 8.63 and 13.2 MPa, and almost double (between 15.2 and 16.2 MPa) at curing 30 days. The CPZ13a sample from Romana, which displayed only a moderate reactive (Table 6), showed a significantly lower mechanical compressive strength than the CPZ11a sample, with values ranging between 0.31 and 0.45 MPa after 20 days from packaging and between 1.19 and 1.25 MPa after curing 30 days. The CPZ13bS sample (also from Romana), which had low Chapelle reactivity values (Table 6), showed even lower resistance values (< 0.75 MPa) even after 30 days (Table 7). The flexural tests show a physical-mechanical behaviour of the four selected samples similar to that of compression. Therefore, the pyroclastic pozzolans of Fordongianus and the perlitic ones of Monte Arci, which for different reasons showed a high reactivity with calcium hydroxide $Ca(OH)_2$, gave the packaged mortars good physical-mechanical characteristics, with fairly high resistance values in the compression and flexural tests of the various specimens performed. The mechanical resistance, over 1 month, is

determined primarily by the carbonation process of the hydrated lime that typically continues in the following months.

The results clearly demonstrate that, with identical mixing proportions, the use of a more reactive pozzolan significantly enhances the performance of the mortars. This highlights that, during the initial phase of curing (spanning over a few months), the reaction at the interface between the pozzolan granules and the hydrated lime creates strong chemical and physical adhesion, leading to improved resistance to mechanical stresses.

It is possible that, over time, once the mortars are exposed to atmospheric conditions, factors such as the partial pressure of water vapour and the circulation of rainwater-derived solutions could reactivate the pozzolanic reaction. This may occur through a slow, but repeated, dissolution of the carbonate component or the reintegration of uncarbonated hydrated lime into the system, leading to renewed chemical-physical interactions with the volcanic aggregate or additive. This chemical-physical process is repeated copiously especially after centuries, as in the case of ancient pozzolanic mortars, as documented by the literature for Roman mortars; some authors [77–79] have in fact highlighted the exceptional performances (in terms of resilience and longevity) of the cementing pozzolanic fabrics of these materials used in the architectural monuments in Rome and marine harbour structures from the Mediterranean region.

In the near future, the chemical-physical and mechanical behaviour of the most reactive volcanic rocks (i.e., CPZ5 and CPZ11a, from the Monte Sparau perlite and Fordongianus pyroclastite quarries, respectively) will be investigated to better guide their use as pozzolans in the production of various low-impact mortars with different technical functions in civil and industrial constructions. This follow-up study will focus on key aspects such as the relationships between chemical reactivity and porosity, specific surface area, and grain size of the pozzolanic aggregate, with the aim of optimising the pozzolanic properties of volcanic rocks and improving mortar performance.

6. Conclusions

The results indicate that the reactivity of the studied pozzolans with hydrated lime, in a strongly alkaline solution (pH about 11.2), varies significantly based on their compositional and microstructural features, which are partly influenced by the volcanic emplacement processes. The main factors affecting reactivity include:

- structure, weight fraction and degree of hydration of the glassy matrix,
- microporosity and specific surface area,
- alteration degree of the rock (subordinately).

Moreover, additional factors with a lesser influence include: (iv) the porphyritic nature (*e.g.*, phenocryst amount, distribution, and size) and (v) the microcrystallinity and texture of the groundmass (*e.g.,* size and distribution of microliths). As evidenced by the Chapelle test results, volcanic rocks with high glass/crystallinity ratio react optimally with lime. Samples with intermediate or poor reactivity have medium-low glass content or show a large mineralogical variability. The most reactive samples are the Monte Arci perlites, which have a glassy microstructure with characteristic concentrically trending micro-cracks at both the submillimeter and sub-micrometer scales, and which show no alteration. The glass hydration process of the vulcanites, induced during syngeneic phase rock cooling by interaction with circulating fluids, acts oppositely: on the one hand, micro-cracking facilitates the formation of interconnected microporosity (and thus reactivity), and on the other hand, it triggers the alteration process with formation of secondary crystalline phases that hinder reactivity. He-porosity of pozzolans does not show a clear correlation with reactivity to hydrated lime; however, the microporosity observed by SEM ($\varnothing<10$ μm), although not related to He-porosity, favors reactivity, as it is closely correlated with specific surface area and it represents the surface exposed to reaction with hydrated lime. Samples with high diffuse microporosity and reactivity are the Fordongianus pumice-cineritic pyroclastites, which being fall deposits show a medium to low degree of welding, with a microstructure that has been preserved following deposition, allowing the formation of inter-particle glassy and crystalline porosities at the microscale.

The chemical and mineralogical alteration of rocks negatively affect reactivity by promoting the formation of secondary phases (such as zeolites, clay-minerals and carbonates), which are typically more stable, thereby reducing the glass/crystal ratio. It is probable, albeit in a subordinate way, that even the variable mineralogical association affected the chemical reactivity. The presence of zeolites in both pyroclastites and perlitic facies, especially at high concentrations (>40 wt%), significantly reduces reactivity. Perlites from the same outcrop containing highly reactive, glassy perlites exhibit good reactivity with hydrated lime, whereas those with a devitrified matrix and secondary minerals (*e.g.*, Ca-erionite) show no reactivity. Overall, this study confirmed that there are several volcanic lithologies in Sardinia that can be exploited as MAPs. Mechanical strength tests on mortars made with pozzolans from Fordongianus and Mount Arci (Morgongiori) demonstrate good performance that improve over time. The primary factor contributing to this strength is the carbonation of calcium hydroxide. However, SEM-EDS analyses also reveal the presence of Si and Al at the binder-pozzolan interface, indicating a chemical exchange occurring at this boundary.

The research results show that most of the waste volcanic materials from the selected quarries, although exhibiting varying degrees of chemical reactivity with the lime-based binder, display pozzolanic behaviour and can therefore be sustainably reused as finely ground aggregates in the production of environmental low-impact mortars. In particular, the physical and mechanical performance of mortars made with Fordongiuanus pyroclastites, Mount Arci perlites, to a lesser extent, with volcanic rocks from Romana, Osilo and Mores volcanic rocks, is promising and warrants further investigation aimed at developing and testing optimal mix designs for various applications in the construction materials industry.

CRediT authorship contribution statement

Dario Fancello: Writing – review & editing, Methodology, Investigation, Formal analysis, Data curation. **Sara Marrocu:** Investigation, Formal analysis. **Stefano Columbu:** Writing – review & editing, Writing – original draft, Visualization, Validation, Supervision, Resources, Methodology, Investigation, Formal analysis, Data curation, Conceptualization. **Concetta Rispoli:** Writing – review & editing. **Piergiulio Cappelletti:** Writing – review & editing. **Giacomo Diego Gatta:** Writing – review & editing, Investigation, Formal analysis. **Giovanni Brodu:** Writing – review & editing, Investigation, Data curation. **Davide Comboni:** Writing – review & editing, Investigation, Formal analysis, Data curation.

Declaration of Competing Interest

The authors declare the following financial interests/personal relationships which may be considered as potential competing interests: Stefano Columbu reports was provided by University of Cagliari. nothing If there are other authors, they declare that they have no known competing financial interests or personal relationships that could have appeared to influence the work reported in this paper.

Acknowledgements

The authors acknowledge support from the University of Cagliari under Open Access funding call for the publication of this work through “DR_344_2025_Avviso_Premialità_OA_Giovani_ricercatori”; author receiving open access funding: Giovanni Brodu, giovanni.brodu@unica.it, ORCID: 0009-0004-8425-3204.

Data availability

Data will be made available on request.

References

[1] M.J. McCarthy, T.D. Dyer, Pozzolanas and pozzolanic materials, Lea'S. Chem. Cem. Concr. 5 (2019) 363–467.
[2] M. Theodoridou, I. Ioannou, M. Philokyprou, New evidence of early use of artificial pozzolanic material in mortars, J. Archaeol. Sci. 40 (8) (2013) 3263–3269.
[3] C.J. Brandon, J.P. Oleson, M.D. Jackson, R.L. Hohlfelder, Building for eternity: the history and technology of roman concrete engineering in the sea. 10, Oxford OX1 2EW, Oxbow Books, UK, 2014. ISBN 978-1-78297-421-5.
[4] M.S. Djerad, K. Boufenara, J. Des Courtils, N. Cantin, Y. Lefrais, Multianalytical characterisation and provenance investigation of natural pozzolana in roman lime mortars from the archaeological site of hippo regius (Algeria), Mediterr. Archaeol. Archaeom. 22 (3) (2022) 231–248.
[5] R. Siddall, The use of volcaniclastic material in roman hydraulic concretes: a brief review, Geol. Soc. Lond. Spec. Publ. 171 (1) (2000) 339–344.
[6] A. Palomo, P. Monteiro, P. Martauz, V. Bílek, A. Fernandez-Jimenez, Hybrid binders: a journey from the past to a sustainable future (opus caementicium futurum), Cem. Concr. Res. 124 (2019) 105829.
[7] L. Medeghini, L. Calzolari, M. Botticelli, M. Di Fazio, C. De Vito, I. Pettiti, F. Bardelli, S. Mignardi, The secret of ancient roman hydraulic mortar: the lesson learnt from the past for future cements, Cem. Concr. Compos. 148 (2024) 105484.
[8] S. Columbu, F. Antonelli, M. Lezzerini, D. Miriello, B. Adembri, A. Blanco, Provenance of marbles used in the heliocaminus baths of hadrian's villa (Tivoli, Italy), J. Archaeol. Sci. 49 (2014) 332–342, https://doi.org/10.1016/j.jas.2014.05.026.
[9] S. Columbu, F. Sitzia, G. Verdiani, Contribution of petrophysical analysis and 3D digital survey in the archaeometric investigations of the emperor Hadrian's baths (Tivoli, Italy), Rend. Lince.. 26 (2015) 455–474, https://doi.org/10.1007/s12210-015-0469-3.
[10] S. Columbu, F. Sitzia, G. Ennas, The ancient pozzolanic mortars and concretes of heliocaminus baths in hadrian's villa (Tivoli, Italy), Archaeol. Anthropol. Sci. 9 (2017) 523–553, https://doi.org/10.1007/s12520-016-0385-1.
[11] S. Columbu, C. Lisci, F. Sitzia, G. Lorenzetti, M. Lezzerini, S. Pagnotta, S. Raneri, S. Legnaioli, V. Palleschi, G. Gallello, B. Adembri, Mineralogical, petrographic and physical-mechanical study of roman construction materials from the maritime theatre of Hadrian's villa (Rome, Italy), Measurement 127 (2018) 264–276, https://doi.org/10.1016/j.measurement.2018.05.103.
[12] B. Liguori, F. Iucolano, B. De Gennaro, M. Marroccoli, D. Caputo, Zeolitized tuff in environmental friendly production of cementitious material: chemical and mechanical characterization, Constr. Build. Mater. 99 (2015) 272–278.
[13] B. Uzal, L. Turanl, B. Yücel, M.C. Göncüoğlu, A. Çulfaz, Pozzolanic activity of clinoptilolite: a comparative study with silica fume, Fly ash and a non-zeolitic natural pozzolan, Cem. Concr. Res. 40 (2009) 398–404.
[14] R. Vigil, Villa de la, R. Fernández, O. Rodríguez, R. García, E. Villar-Cociña, M. Frías, Evolution of the pozzolanic activity of a thermally treated zeolite, J. Mater. Sci. 48 (8) (2013) 3213–3224, https://doi.org/10.1007/s10853-012-7101-z.
[15] G. Mertens, R. Snellings, B. Van Balen, B. Simsir, P. Verlooy, J. Elsen, Pozzolanic reactions of common natural zeolites with lime and parameters affecting their reactivity, Cem. Concr. Res. 39 (2009) 233–240.
[16] R. Snellings, G. Mertens, J. Elsen, Supplemental cementitious materials, Rev. Mineral. Geochem. 74 (2012) 211–278.
[17] A. Moropoulou, A. Bakolas, K. Bisbikou, Investigation of the technology of historic mortars, J. Cult. Herit. 1 (2000) 45–58.
[18] J. Lanas, J.L.P. Bernal, M.A. Bello, J.I. Alvarez Galindo, Mechanical properties of natural hydraulic lime-based mortars, Cem. Concr. Res. 34 (2004) 2191–2201.
[19] S. Columbu, M. Lezzerini, G. Verdiani, Geochemical and petrographic analysis on the stones and integrated digital survey of the cathedral of Sant'Antioco di bisarcio (Ozieri, Italy). Metrology for Archaeology and Cultural Heritage, IEEE International Conference on, 2018, pp. 117–122, https://doi.org/10.1109/MetroArchaeo43810.2018.13603. MetroArchaeo Proceedings 2018.
[20] M. Lezzerini, S. Raneri, S. Pagnotta, S. Columbu, G. Gallello, Archaeometric study of mortars from the pisa's cathedral square (Italy), Measurement 126 (2018) 322–331, https://doi.org/10.1016/j.measurement.2018.05.057.
[21] S. Raneri, S. Pagnotta, M. Lezzerini, S. Legnaioli, V. Palleschi, S. Columbu, N.F. Neri, P. Mazzoleni, Examining the reactivity of volcanic ash in ancient mortars by using a micro-chemical approach, Mediterr. Archaeol. Archaeom. 18 (2018) 147–157, https://doi.org/10.5281/zenodo.1285897.
[22] C. Rispoli, G. Montesano, M. Verde, V. Morra, P. Cappelletti, The key to ancient roman mortars hydraulicity: ceramic fragments or volcanic materials? A lesson from the phlegrean archaeological area (Southern Italy), Constr. Build. Mater. 411 (2024) 134408.
[23] A. Alujas, R. Fernández, R. Quintana, K.L. Scrivener, F. Martirena, Pozzolanic reactivity of lowgrade kaolinitic clays: influence of calcinations temperature and impact of calcination products on OPC hydration, Appl. Clay Sci. 108 (2015) 94–101.

[24] W. Hermann, J. Tchamdjou, S. Grigoletto, F. Michel, L. Courard, T. Cherradi, M. Larbi, Abidi, Effects of various amounts of natural pozzolans from volcanic scoria on performance of portland cement mortars, Int. J. Eng. Res. Afr. 32 (2017) 36–52.
[25] M. Stefanidou, Use of natural pozzolans with lime for producing repair mortars, Environ. Earth Sci. (2016) 750–758.
[26] M. Hamidi, M. Kacimi, M. Cyr, P. Clastres, Evaluation and improvement of pozzolanic activity of andesite for its use in eco-efficient cement, Constr. Build. Mater. 47 (2013) 1268–1277.
[27] M. Pavlíková, P. Rovnaníková, M. Záleská, Z. Pavlík, Diatomaceous Earth—Lightweight pozzolanic admixtures for repair Mortars—Complex chemical and physical assessmen, Materials 15 (19) (2022) 6881, https://doi.org/10.3390/ma15196881.
[28] P. Segui, J.E. Aubert, B. Husson, M. Measson, Utilization of a natural pozzolan as the main component of hydraulic road binder, Constr. Build. Mater. 40 (2012) 217–223.
[29] E.L. Advokaat, D.J.J. Van Hinsbergen, M. Maffione, C.G. Langereis, R.L.M. Vissers, A. Cherchi, R. Schroeder, H. Madani, S. Columbu, A. Eocene rotation of sardinia, and the paleogeography of the Western Mediterranean region, Earth Planet. Sci. Lett. 401 (2014) 183–195.
[30] A. Cherchi, L. Montadert, Oligo-Miocene rift of sardinia and the early history of the Western Mediterranean basin, Nature 298 (1982) 736–739.
[31] Coulon, C. 1977. Le volcanism calco-alcalin cenozoique de Sardaigne, Italie. Unpublished master's thesis, Univesité St. Jerome, Marseille.
[32] J. Dostal, C. Coulon, C. Dupuy, Cainozoic andesitic rock of sardinia (Italy), in: R.S. Thorpe (Ed.), Andesites: orogenic andesites and related rocks, J. Wiley & Sons, Chichester, 1982, pp. 353–370.
[33] C. Faccenna, F. Speranza, F.D.A. Caracciolo, M. Mattei, G. Oggiano, Extensional tectonics on sardinia (Italy): insights into the arc–back-arc transitional regime, Tectonophysics 356 (4) (2002) 213–232.
[34] L. Beccaluva, G. Bianchini, C. Natali, F. Siena, Geodynamic control on orogenic and anorogenic magmatic phases in sardinia and Southern Spain: inferences for the cenozoic evolution of the Western Mediterranean, Lithos 180 (181) (2011) 128–137.
[35] J. Burrus, Contribution to a geodynamic synthesis of the provencal basin. (NW Mediterranean), Mar. Geol. 55 (1984) 247–269.
[36] A. Cherchi, N. Mancin, L. Montadert, M. Murru, M.T. Putzu, F. Schiavinotto, V. Verrubbi, The stratigraphic response to the Oligo-Miocene extension in the Western Mediterranean from observations on the sardinia graben system (Italy), Bull. De. la Soc. Geol. De. Fr. 179 (2008) 267–287.
[37] L. Beccaluva, G. Bianchini, M. Coltorti, F. Siena, M. Verde, Cenozoic Tectono- magmatic evolution of the Central-Western Mediterranean: migration of an Arc-interarc basin system and variations in the mode of subduction, in: I. Finetti (Ed.), Elsevier Special Volume, "Crop Project — Deep Seismic Exploration of the Central Mediterranean and Italy, 2005, pp. 623–640.
[38] L. Beccaluva, G. Bianchini, C. Bonadiman, M. Coltorti, G. Macciotta, F. Siena, C. Vaccaro, Within-plate cenozoic volcanism and lithospheric mantle evolution in the Western-Central Mediterranean area, in: I. Finetti (Ed.), Crop Project — Deep Seismic Exploration of the Central Mediterranean and Italy, Elsevier Special Volume, 2005, pp. 641–664.
[39] M. Lustrino, S. Duggen, C.L. Rosenberg, The Central-Western Mediterranean: anomalous igneous activity in an anomalous collisional tectonic setting, Earth Sci. Rev. 104 (2011) 1–40.
[40] S. Columbu, Petrographic and geochemical investigations on the volcanic rocks used in the Punic-Roman archaeological site of nora (Sardinia, Italy), Environ. Earth Sci. 77 (2018) 577, https://doi.org/10.1007/s12665-018-7744-4.
[42] M. Lustrino, V. Morra, L. Fedele, L. Franciosi, Beginning of the apennine subduction system in central Western Mediterranean: constraints from cenozoic "orogenic'' magmatic activity of sardinia, Italy, Tectonics 28 (2009). TC5016.
[42] R. Montigny, J.B. Edel, R. Thuizat, Oligo-miocene rotation of sardinia: k-ar ages and paleomagnetic data of tertiary volcanics. Earth and planet, Sci. Lett. 54 (1981) 261–271.
[43] L. Beccaluva, L. Civetta, G. Macciotta, C.A. Ricci, Geochronology in sardinia: results and problems, Rend. Soc. It. Min. Petr 40 (1985) 57–72.
[44] C. Savelli, Datazioni preliminari col metodo K-Ar di vulcaniti della sardegna sud-occidentale, Rend. Soc. It. Min. Petr 31 (1975) 191–198.
[45] E. Carminati, C. Doglioni, Alps vs. Apennines: the paradigm of a tectonically asymmetric earth, Earth Sci. Rev. 112 (2012) 67–96.
[46] J. Gattaceca, A. Deino, R. Rizzo, D.S. Jones, B. Henry, B. Beaudoin, F. Vadeboin, Miocene rotation of sardinia: new paleomagnetic and geochronological constraints and geodynamic implications, Earth Planet. Sci. Lett. 258 (2007) 359–377.
[47] F. Speranza, I.M. Villa, L. Sagnotti, F. Florindo, D. Cosentino, P. Cipollari, M. Mattei, Age of the Corsica-Sardinia rotation and Liguro-Provençal basin spreading: new paleomagnetic and Ar/Ar evidence, Tectonophysics 347 (4) (2002) 231–251.
[49] A. Peccerillo, M.L. Frezzotti, Magmatism, mantle evolution and geodynamics at the converging plate margins of Italy, JCS 172 (2015) 407–427.
[50] M. Lustrino, L. Melluso, V. Morra, The role of lower continental crust and lithospheric mantle in the genesis of Plio-Pleistocene volcanic rocks from sardinia (Italy), Earth Planet. Sci. Lett. 180 (3-4) (2000) 259–270, 2000.
[51] A. Assorgia, L. Beccaluva, G.M. Di Paola, L. Maccioni, G. Macciotta, M. Puxeddu, R.And Santacroce, G. Venturelli, Il complesso vulcanico di monte arci (Sardegna centro- occidentale), Nota Illus. alla Carta geopetrografica 150. 000. Boll. Soc. Geol. It 95 (1976) 371–401.
[52] L. Beccaluva, M. Deriu, L. Maccioni, G. Macciotta, G. Venturelli, II massiccio vulcanico di monte arci (Sardegna centro occidentale), Rend. Soc. Ital. Mineral. Petrogr. 30 (1974) 1069–1081.
[53] A. Assorgia, K. Balogh, L. Lecca, A. Ibba, A. Porcu, F. Secchi, G. Tilocca, Volcanological characters and structural context of Oligo-Miocene volcanic succession from central sardinia (Italy), Acc.Naz. delle sc. XL.XIV Rapp. AlpiAppennino 1994 (1995) 397–424.
[54] A. Assorgia, L. Beccaluva, G.M. Di Paola, L. Maccioni, G. Macciotta, M. Puxeddu, R. Santacroce, G. Venturelli, Il complesso vulcanico di monte arci (Sardegna centro-occidentale): nota illustrativa alla carta geopetrografica 1:50.000, Boll. Soc. Geol. It. 95 (1976) 371–401.
[55] A. Assorgia, S. Barca, C. Spano, A syntehesis on the cenozoic stratigraphic, tectonic and volcanic evolution in sardinia (Italy), Boll. Soc. Geol. It. 116 (1997) 407–420.
[56] L. Lecca, R. Lonis, S. Luxoro, F. Melis, F. Secchi, P. Brotzu, Oligo miocene volcanic sequences and rifting stages in sardinia: a review, Per. Miner. 66 (1997) 7–61.
[57] L. Beccaluva, M. Coltorti, B. Galassi, G. Macciotta, F. Siena, The cainozoic calcalkaline magmatism of the Western Mediterranean and its geodynamic significance, Boll. di Geofis. Teor. Ed. Appl. 36 (1994) 141–144.
[58] Larson, A.C.; Von Dreele, R.B. General Structure Analysis System "GSAS"; Los Alamos National Laboratory: Los Alamos, NM, USA, 1994.
[59] B.H. Toby, EXPGUI, a graphical user interface for GSAS, J. Appl. Crystallogr 34 (2001) 210–213.
[60] A.F. Gualtieri, G.D. Gatta, R. Arletti, G. Artioli, P. Ballirano, G. Cruciani, A. Guagliardi, D. Malferrari, N. Masciocchi, P. Scardi, Quantitative phase analysis using the rietveld method: towards a procedure for checking the reliability and quality of the results, Period. Miner. 88 (2019) 147–151.
[61] UNI EN 196-1:2016, Metodi di prova dei cementi - Parte 1: Determinazione delle resistenze Meccaniche.
[62] S. Columbu, G. Cruciani, D. Fancello, M. Franceschelli, G. Musumeci, Petrophysical properties of a granite-protomylonite-ultramylonite sequence: insight from the monte grighini shear zone, central sardinia, Italy, Eur. J. Miner. 27 (2014) 471–486, https://doi.org/10.1127/ejm/2015/0027-2447.
[63] C. Buosi, S. Columbu, G. Ennas, P. Pittau, G.G. Scanu, Mineralogical, petrographic, and physical investigations on fossiliferous middle jurassic sandstones from central sardinia (Italy) to define their alteration and experimental consolidation, Geoheritage 11 (2019) 729–749, https://doi.org/10.1007/s12371-018-0326-8.
[64] S. Columbu, M. Mulas, F. Mundula, R. Cioni, Strategies for helium pycnometry density measurements of welded ignimbritic rocks, Meas. J. Int. Meas. Confed. 173 (2021) 108640, https://doi.org/10.1016/j.measurement.2020.108640.
[65] ISRM, International Society For Rock Mechanics, Suggest method for determining the point load strength. Isrm commis- sion for testing methods, working group on revision of the point load test methods, in: Int J Rock Mech Min Sci Geomech Abstr, 22, 1985, pp. 51–60.
[66] P. Cappelletti, G. Cerri, M. de Gennaro, A. Langella, S. Naitza, G. Padalino, M. Palomba, R. Rizzo, 01-O-02-Natural zeolites mineralization in the Oligocene-Miocene volcano-sedimentary succession of central sardinia (Italy), Stud. Surf. Sci. Catal. 135 (2001) 147.
[67] M. Palomba, G. Padalino, M. Marchi, Industrial mineral occurrences associated with cenozoic volcanic rocks of sardinia (Italy): geological, mineralogical, geochemical features and genetic implications, Ore Geol. Rev. 29 (2) (2006) 118–145, https://doi.org/10.1016/j.oregeorev.2005.11.008.
[68] L.N. Warr, IMA–CNMNC approved mineral symbols, Mineral. Mag. 85 (2021) 291–320, https://doi.org/10.1180/mgm.2021.43.
[69] O. Jankovský, Z. Pavlík, M. Záleská, M. Pavlíková, A. Pivák, J. Nábělková, A.M. Lauermannová, A. Jiříčková, D. Sedmidubský, Fly ash admixture originating from lignite combustion in construction mortars – time evolution of technical parameters and heavy metals leachability, Results Eng. 24 (2024) 102945.

[70] T. Perraki, A. Orfanoudaki, Mineralogical study of zeolites from pentalofos area, thrace, Greece, Appl. Clay Sci. 25 (1-2) (2004) 9–16.
[71] M. Sprynskyy, R. Golembiewski, G. Trykowski, B. Buszewski, Heterogeneity and hierarchy of clinoptilolite porosity, J. Phys. Chem. Solids 71 (9) (2010) 1269–1277.
[72] M. Król, J. Dechnik, P. Szymczak, B. Handke, M. Szumera, P. Stoch, Thermal behavior of clinoptilolite, Crystals 14 (7) (2024) 646.
[73] T. Perraki, G. Kakali, E. Kontori, Characterization and pozzolanic activity of thermally treated zeolite, J. Therm. Anal. Calor. 82 (2005) 109–113, https://doi.org/10.1007/s10973-005-0849-5.
[74] Ö.Ç. Duvarcı, Y. Akdeniz, F. Özmıhçı, S. Ülkü, D. Balköse, M. Çiftçioğlu, Thermal behaviour of a zeolitic tuff, Ceram. Int. 33 (2007) 795–801, https://doi.org/10.1016/j.ceramint.2006.01.003.
[75] P.M. Angelopoulos, N. Manic, B. Jankovic, M. Taxiarchou, Thermal decomposition of volcanic glass (rhyolite): kinetic deconvolution of dehydration and dehydroxylation process, Thermochim. Acta 707 (2022) 179082.
[76] R. Cioni, G. Macciotta, M. Marchi, G. Padalino, R. Simeone, M. Palomba, Water-rock interaction in genesis of perlite at monte arci volcanic complex (West Sardinia, Italy), proceedings of the "10th international symposium, Water Rock. Interact." (WRI 10) (2001) 693–696. Villasimius (Cagliari, Italy), 10-15 June, 2001.
[77] M.D. Jackson, S.R. Mulcahy, H. Chen, Y. Li, Q. Li, P. Cappelletti, H.R. Wenk, Phillipsite and Al-tobermorite mineral cements produced through low-temperature water-rock reactions in roman marine concrete, Am. Mineral. 102 (2017) 1435–1450, 2017.
[78] M.D. Jackson, J.P. Oleson, J. Moon, Y. Zhang, H. Chen, M.T.F. Gudmundsson, Extreme durability in ancient roman concretes, Am. Ceram. Soc. Bull. 97 (5) (2018) 22–28.
[79] J. Elsen, M.D. Jackson, E. Ruiz-Agudo, Historic concrete science: opus caementicium to "Natural cements, 2022, Elements 18 (5) (2022) 301–307.
[47] M. Lustrino, V. Morra, L. Fedele, M. Serracino, The transition between 'orogenic' and 'anorogenic' magmatism in the Western Mediterranean area: the middle miocene volcanic rocks of isola del toro (SW Sardinia, Italy), Terra Nova 19 (2) (2007) 148–159, 2007.